ANNULAR MODES OF THE TROPOSPHERE AND STRATOSPHERE

Paul J. Kushner[1]

Reviews of Geophysics, ???, /
pages 1??
8755-1209/10/£15.00
Paper number

Abstract

A pedagogical review of the phenomenology, dynamics and simulation of the Annular Modes is presented. First, the manner in which the Annular Modes capture the principal features of variability in the zonal mean circulation of the extratropical stratosphere and troposphere is demonstrated. Next, elementary ideas about Annular Mode dynamics, in particular the distinct eddy mean-flow interactions that govern the modes in the troposphere and stratosphere, are introduced. The review concludes with a discussion of the representation of the Annular Modes in simplified and comprehensive general circulation models, in the context of stratosphere-troposphere interactions in intraseasonal variability and climate change.

1. INTRODUCTION

For the theory of the atmospheric general circulation it is important to not only account for the circulation's principal climatological features, such as the jet streams of the troposphere and the polar night jet of the stratosphere, but also to develop a dynamical description of how the circulation varies about its climatological mean. In this chapter, we present a pedagogical review of the Annular Modes [hereafter AMs; *Thompson and Wallace*, 2000; *Thompson et al.*, 2000; *Limpasuvan and Hartmann*, 1999, 2000], which are the principal modes of variation of the extratropical circulation of the troposphere and stratosphere on timescales greater than a few weeks. Because much of the observed extratropical variability is manifested in the AMs, explaining their dynamics represents an important theoretical task. Beyond this, the AMs are of applied importance because of their impacts on many climate processes and because of their relationship to climate change signals [e.g. *Shindell et al.*, 1999; *Thompson et al.*, 2000; *Thompson and Solomon*, 2002; *Kushner et al.*, 2001; *Russell and Wallace*, 2004; *Miller et al.*, 2006; *Butler et al.*, 2007].

In this Chapter, we will discuss the observed AMs (Section 2), which consist of the Southern Annular Mode (SAM) in the Southern Hemisphere and the Northern Annular Mode (NAM) in the Northern Hemisphere; present some elementary ideas on their dynamics and their representation in highly simplified models (Section 3); and explore their central role in extratropical climate variability and change, with an emphasis on their behaviour in more complex models (Section 4). We will adopt the viewpoint that the AMs represent coherent variations of the zonal mean circulation that interact with synoptic-to-planetary scale atmospheric waves and the zonal stresses they induce [e.g. *Limpasuvan and Hartmann*, 1999, 2000]. We will find that, despite their importance, the AMs remain enigmatic because they are derived empirically and because there is no simple first-principles theory describing their structure and dynamics in the stratosphere and troposphere. Our current theoretical understanding is instead represented in simplified nonlinear models in which AM structures emerge as the leading modes of variability [e.g. *Vallis et al.*, 2004; *Holton and Mass*, 1976; *Scott and Polvani*, 2006] and in detailed dynamical analyses of their temporal variability [e.g. *Robinson*, 2000; *Lorenz and Hartmann*, 2001, 2003]. In the absence of a predictive theory, and in light of the many ways in which AM responses can be stimulated by climate forcings, we need to rely on comprehensive climate models to quantitatively simulate the AMs and predict their future behaviour under climate change.

Before proceeding, we highlight some of the important papers from the late 1990's and early 2000's that defined the AMs and recognized their significance. These papers represent a starting point for further exploration for the interested student.

• The original description of the AMs as the principal modes of variability of the extratropical circulation, for the stratosphere and the troposphere of both the Northern Hemisphere and Southern Hemisphere; their relationship to the North Atlantic Oscillation; and their impacts on weather variability is primarily due to Thompson and Wallace [see *Thompson and Wallace*, 1998, 2000; *Wallace*, 2000; *Thompson et al.*, 2000; *Thompson and Wallace*, 2001, among other studies]. The principal original work describing the eddy mean-flow interactions that maintain the AMs is that of *Limpasuvan and Hartmann* [1999, 2000] and *Lorenz and Hartmann* [2001, 2003]. This set of studies revitalized a line of work on variability of the zonal mean circulation that dates back several decades. (The historical literature is well referenced in the cited papers.) Regarding terminology, the term "Annular Modes" was first used in *Thompson and Wallace* [2000] (which was received by *J. Climate* in 1998) and *Limpasuvan and Hartmann* [1999] (which was received by *Geophys. Res. Lett.* in 1999). The NAM and SAM were originally named the Arctic Oscillation and the Antarctic Oscillation; these terms are still used in some papers. The relationship between the AMs and the classical zonal index, which is a dipolar mode of variability that corresponds to the tropospheric AM in zonal wind, is detailed in *Wallace* [2000].

• The observational description of the time dependent coupling between stratospheric and tropospheric variability through the daily evolution of the AMs, and its implications for prediction of cli-

[1]Department of Physics, University of Toronto, Canada

mate variability on seasonal timescales, is primarily due to Baldwin, Dunkerton and collaborators [e.g. *Baldwin and Dunkerton*, 1999, 2001; *Baldwin et al.*, 2003]. These papers followed a long line of inquiry that identified influences that the state of the stratosphere might have on the tropospheric circulation, involving both zonal mean and regional circulation features [e.g. *Boville*, 1984; *Kodera et al.*, 1990; *Perlwitz and Graf*, 1995].

• The connection between the Annular Modes and climate change in the extratropics and to Antarctic stratospheric ozone depletion is due to *Thompson and Wallace* [1998]; *Shindell et al.* [1999]; *Fyfe et al.* [1999]; *Thompson et al.* [2000]; *Kushner et al.* [2001]; *Sexton* [2001]; *Thompson and Solomon* [2002]; *Polvani and Kushner* [2002]; *Gillett and Thompson* [2003], among others.

The discovery of the AMs has spurred a large literature that extends well outside the atmospheric and physical climate sciences. We do not provide here a comprehensive review of this literature, but aim to highlight a select set of points intended to introduce the AMs to researchers new to the field.

2. OBSERVED AM STRUCTURE

The AMs are atmospheric *teleconnection patterns* — that is, continental-to-planetary scale patterns involving statistical coherence between spatially remote points — that are derived using a variety of methods [as recently reviewed in *Baldwin and Thompson*, 2009; *Baldwin et al.*, 2009]. Typically, the AMs are derived using empirical orthogonal function (EOF) analysis of selected extratropical meteorological fields. EOF analysis represents a straightforward multivariate statistical approach, but one that risks artificially conflating spatially and dynamically distinct phenomena. In this section, we will show that the AMs indeed represent physically meaningful and statistically robust patterns that connect the zonal mean variability of the troposphere and stratosphere.

Using notation similar to *Baldwin et al.* [2009], EOF analysis decomposes an $n \times p$ data matrix $\mathbf{X}$ consisting of n temporal observations at p points into a series of $n \times p$ matrices according to

$$\mathbf{X} = \sum_{i=1}^{r} \mathbf{y}_i \mathbf{e}_i^T = \mathbf{y}_1 \mathbf{e}_1^T + \mathbf{y}_2 \mathbf{e}_2^T + \ldots + \mathbf{y}_r \mathbf{e}_r^T, \quad (1)$$

where r is the rank of $\mathbf{X}$, which is never greater than the minimum of n and p; $\mathbf{y}_i$ is a column vector representing the ith n-point *principal component* (PC) time series; and $\mathbf{e}_i$ is a column vector representing the ith p-point spatial EOF. The EOFs are the eigenvectors of the $p \times p$ sample covariance matrix $\mathbf{S} = \mathbf{X}^T\mathbf{X}$, and are ranked in descending order of the size of the positive quantity $\mathbf{e}_i^T\mathbf{S}\mathbf{e}_i$ — when divided by the total variance in the field, this quantity is known as the "variance explained" or "represented" by EOF i. The r PC time series $\mathbf{y}_i$ are mutually orthogonal, as are the r EOFs $\mathbf{e}_i$. A spatial pattern associated with another field $\tilde{\mathbf{X}}$ that is coherent with the jth EOF is found by regression according to

$$\tilde{\mathbf{x}}_j = \frac{\tilde{\mathbf{X}}^T \mathbf{y}_j}{\mathbf{y}_j^T \mathbf{y}_j} \quad (2)$$

where $\tilde{\mathbf{X}}$ is an $n \times \tilde{p}$ data matrix consisting of $\tilde{p}$ n-point time series. If we set $\tilde{\mathbf{X}} = \mathbf{X}$, which is the original data matrix, then the spatial pattern that results from (2) is the jth the EOF: $\tilde{\mathbf{x}}_j = \mathbf{e}_j$. The effects of spatial weighting are straightforward to bring into this formalism [*Baldwin et al.*, 2009].

In this notation, the AM EOF corresponds to $\mathbf{e}_1$ for an appropriately chosen $\mathbf{X}$ and the AM index corresponds to the PC time series $\mathbf{y}_1$. To define the AMs, one must choose the meteorological field $\mathbf{X}$ and the way to sample that field in space and time. A review of various approaches [e.g. *Gong and Wang*, 1999; *Thompson and Wallace*, 2000; *Wallace*, 2000; *Baldwin*, 2001; *Lorenz and Hartmann*, 2001; *Monahan and Fyfe*, 2006; *Kushner and Lee*, 2007], not all of which use EOF analysis as the basis for the AM index [e.g. *Gong and Wang*, 1999], shows that the different methods yield similar results in the sense that the resulting AM indexes are strongly temporally correlated. But this similarity can mask systematic underlying differences: for example, *Monahan and Fyfe* [2006] show that the meridional structure of the AM defined using geopotential height differs from that using geostrophic wind because the loading pattern of variance for a field differs from the loading pattern for the field's spatial gradient. Focussing on the vertical structure, *Baldwin and Thompson* [2009] show that the choice of input field affects the manner in which stratosphere-troposphere coupling (see below) is manifested on short timescales.

To help understand the nature of the variance represented by the AMs, we examine the spatial and temporal structure of extratropical zonal mean variability to be captured by the EOF analysis. We start with the zonal mean geopotential $\overline{Z} = \overline{Z}(\theta, p, t)$, where the overbar indicates a zonal mean and (θ, p, t) are latitude, pressure and time. We then remove its climatological mean; call this quantity Z^a, where the superscript a indicates an anomaly from the climatology. We then define

$$\tilde{Z}(\theta, p, t) = \overline{Z^a}(\theta, p, t)\sqrt{\cos\theta}, \quad (3)$$

which, after some further processing, will provide the input to the EOF calculation. The geometric factor $\sqrt{\cos\theta}$ relates to the cosine-latitude weight-

ing within the inner product for the EOF calculation [*Baldwin et al.*, 2009]; we will for this analysis retain it in the definition of $\tilde{Z}$ and now examine $\tilde{Z}$ as a measure of variability in the zonal mean circulation.

We first show the periodogram (i.e. the discrete Fourier temporal spectrum) of $\tilde{Z}$ as a function of latitude from South Pole to North Pole and of timescale from weeks to years for the lower troposphere in Plate 1a and for the lower stratosphere in Plate 1b. We also show the extratropical meridional mean of these spectra in Plate 1c. While the variance of $\tilde{Z}$ from (3), by construction, goes to zero at the poles, the variance of $\overline{Z^a}$ amplifies to a maximum at the poles (not shown). Because for timescales shorter than annual geopotential variance is generally stronger in the extratropics than the tropics (as expected from geostrophic balance), the definition of the AMs is relatively insensitive to the equatorial extent of the domain of analysis [see e.g. *Baldwin and Thompson*, 2009]. In the troposphere, there is a broad band of variance poleward of about 30 degrees latitude and a suggestion of a minimum in variance around 60 degrees latitude in each hemisphere. Plate 1c shows that in the troposphere the variance has for the most part saturated on timescales longer than the intraseasonal (multiple-week) timescale. In the stratosphere, the variance is relatively strong at higher latitudes, and shifted to longer timescales; the variance continues to build up beyond intraseasonal timescales. The structure in latitude and frequency is similar in both hemispheres, suggesting that the dynamics of the AMs in each hemisphere might be dynamically similar. This hemispheric symmetry is less evident for zonal wind than for $\tilde{Z}$ (not shown).

We now examine the seasonal dependence of the variability of the zonal mean circulation represented by $\tilde{Z}$. We calculate the monthly mean $\tilde{Z}$, remove that part of the result that is linearly coherent with the Monthly ENSO Index [MEI defined by *Wolter and Timlin*, 1993, see *Lorenz and Hartmann*, 2003], linearly detrend this result, and from this last result create seasonal time series for three sequential months each year. (For example, we create a time series of the months January-February-March for each year from 1979 to 2008, representing a three month "JFM" season, yielding a 90-record time series.) We denote by $\tilde{Z}_{\rm mon}$ the result of this sequence of operations on $\tilde{Z}$. This captures seasonal and longer timescale variability and eliminates submonthly variability, for which, from Plate 1, the variability can be seen to be far from saturation.

We show the seasonal cycle of the standard deviation of monthly mean $\tilde{Z}_{\rm mon}$ in the extratropics, as a function of center month (Februrary in the previous example) in Plate 2, for lower tropospheric, upper tropospheric, and lower stratospheric levels. The ENSO filtering removes variance at low latitudes (not shown). In the troposphere of both hemispheres, $\tilde{Z}_{\rm mon}$ has a strong wintertime maximum in the higher extratropics and a weaker maximum in the lower extratropics. These features are vertically aligned, suggesting that the underlying variability might be equivalent barotropic in the troposphere. The seasonal cycle is more pronounced in the Northern Hemisphere troposphere than in the Southern Hemisphere troposphere. The maximum in variance in the Southern Hemisphere troposphere arrives in late fall, earlier in the season than the corresponding maximum in the Northern Hemisphere troposphere. In the Northern Hemisphere stratosphere, the maximum variance is found in the winter but in the Southern Hemisphere stratosphere, the maximum variance is delayed towards the spring. The period of maximum variance in the stratosphere represents the *active season* of the stratospheric polar vortex in each hemisphere, when the polar stratospheric winds are eastward and display considerable variability; this season is delayed towards spring in the Southern Hemisphere [*Thompson and Wallace*, 2000; *Hartmann et al.*, 2000].

Plates 1-2 represent the variability that the AMs, as leading modes, should capture. To calculate the AMs, we set $\mathbf{X} = \tilde{Z}_{\rm mon}(|\theta| > 20^0, p = 850 \text{ hPa}, t)$ in (1), i.e. we use extratropical lower tropospheric $\tilde{Z}_{\rm mon}$ as input to the EOF analysis [*Thompson and Wallace*, 2000]. The NAM and SAM are the leading EOFs in the Southern Hemisphere and Northern Hemisphere. We repeat this calculation for each calendar month and for each hemisphere. Plate 3 plots the regression of the AMs on $\tilde{Z}_{\rm mon}$, using (2), for the same vertical levels as in Plate 2. These are the patterns of variability coherent with the lower-troposphere based AM in its positive phase at each level, for each calendar month and for each hemisphere.

Comparing Plates 2 and 3, which have equivalent contour intervals in each panel, we see that the leading EOF captures the principal features of the variance and its seasonal cycle throughout the troposphere and stratosphere, even though the AM definition involves only information from the lower troposphere. The tropospheric AM EOF consists of a dipolar structure in $\tilde{Z}_{\rm mon}$ that reflects the high-extratropical and low-extratropical maxima in variance in the two hemispheres and the broad band of variance seen in Plate 1a. During the active season when the variance is large in the lower stratosphere, the AM anomaly pattern has a consistent sign between the stratosphere and the troposphere poleward of 60^0 latitude. This verti-

cal coherence indicates that the stratosphere and troposphere are coupled in the active season.

Despite the evidence of coupling between the stratosphere and troposphere, Plate 3 also suggests that the main features of the tropospheric AM structure appear to be independent of the stratosphere. In particular, the dipolar tropospheric AM in Plate 3 persists throughout most of the year, especially in the Southern Hemisphere. The stratospheric AM, on the other hand, is strongly amplified during the active stratospheric season and is strongly attenuated in the inactive season when the stratospheric winds are easterly. This implies, as will be discussed in Section 3, that to some extent the dynamics of the stratospheric and tropospheric AM are distinct and can be considered separately.

During the active season, when the variability of the stratosphere and troposphere is vertically coherent, the NAM and SAM are remarkably hemispherically symmetric [*Thompson and Wallace*, 2000]. Plate 4 shows the 850 hPa SAM and NAM signatures in the zonal wind (that is, $\tilde{\mathbf{X}}$ corresponds to $\overline{u}$ in (2), where $\overline{u}$ is the zonal mean zonal wind). In the troposphere, the AM in the wind in each hemisphere is strongly dipolar while in the stratosphere the AM is more monopolar. Although the node of the SAM is located a few degrees poleward of the node of the NAM, the patterns essentially represent a reflection of each other across the equator. To quantify the hemispheric symmetry, we also show the associated hemispherically symmetric component of the patterns, $\overline{u}_{\rm sym}$, which is obtained by first reflecting SAM pattern $\overline{u}_{\rm SAM}$ and then averaging it with the NAM pattern $\overline{u}_{\rm NAM}$:

$$\overline{u}_{\rm sym}(y) = \frac{1}{2}[\overline{u}_{\rm SAM}(-y) + \overline{u}_{\rm NAM}(y)],$$

where y is the Cartesian meridional coordinate that we will use in the rest of the Chapter. The symmetric component explains 96% of the variance in the AMs (using a log-pressure weighting poleward of 10 degrees latitude), and the symmetric pattern looks quite similar to both the SAM and the NAM. Applying such a construction to the zonal mean wind in each hemisphere (bottom row of Plate 4) does not give the same qualitative sense of hemispheric symmetry: the Northern Hemisphere jet is dominated by the subtropical jet, while the Southern Hemisphere jet structure is more split between its subtropical and extratropical parts; the Northern Hemisphere surface jet is not as sharp, and the stratospheric jet is relatively weak. (The resulting symmetric component [bottom right panel of Plate 4] explains 88% of the variance of the total wind.)

The fact that the AMs are more hemispherically symmetric than the background circulation (as is also found for the tropospheric AMs outside the active season — not shown) suggests that the AMs are governed by dynamics that does not depend highly on the meridional structure of the background flow. It also means that the spatial relationship between the jets and the AMs is distinct in each hemisphere. In the Southern Hemisphere, the tropospheric jet maximum at each altitude (red solid line in the upper left panel of Plate 4) is located along the node of the SAM; the SAM in its positive phase thus describes a poleward shift of the jet. Given a shift δy of the jet, we expect a wind anomaly that is related to the vorticity of the jet according to

$$\overline{u}_{\rm SAM} \sim \overline{u}(y - \delta y) - \overline{u}(y) \approx -\delta y\, \overline{u}_y = \delta y\, \overline{\zeta},$$

where $\overline{u}(y)$ represents the tropospheric jet profile as a function of meridional coordinate y, where coordinate subscripts indicate partial derivatives, and where $\overline{\zeta} = -\overline{u}_y$ is the zonal mean vorticity of the jet. This relationship suggests that spatial scale of the tropospheric SAM is linked to the spatial scale of the barotropic shear, i.e. of the vorticity of the jet, and the amplitude of the SAM to the degree of displacement of the jet. Taking extratropical tropospheric vorticity values of $\overline{\zeta} \sim 10^{-5}\,{\rm s}^{-1}$ and $\overline{u}_{\rm SAM} \sim 1 - 2\,{\rm m\,s}^{-1}$ for the SAM in the troposphere suggests that typical seasonal-to-interannual SAM fluctuations are related to seasonal-to-interannual variations in the position of the jet of about $\delta y \sim \overline{\zeta}/\overline{u}_{\rm SAM} \sim 100 - 200\,{\rm km}$; climate trends discussed in Section 4 correspond to tropospheric jet shifts of this magnitude [*Kushner et al.*, 2001]. The relationship between the jet position and the SAM node holds at each longitude, when the regional structure of the SAM is analyzed [*Codron*, 2005]. In the stratosphere, the jet axis is aligned with the maximum of the SAM. Thus, in the Southern Hemisphere active season, the SAM in its positive phase is described as a poleward shift of the tropospheric jet and a strengthening of the stratospheric polar vortex.

This empirical description for the Southern Hemisphere does not generalize simply to the Northern Hemisphere. In the Northern Hemisphere, the relationship between the stratospheric vortex and the NAM is similar to that for the Southern Hemisphere (see red lines in Plate 4b). But in the troposphere, positive NAM conditions consist of a reduction in strength of the subtropical jet and an intensification on the poleward side of the jet, rather than a simple poleward shift of the jet. Thus we do not find a simple connection between the barotropic shear of the zonal mean wind and the tropospheric NAM structure. The relationship between the Northern Hemisphere jet stream and the NAM varies regionally: in the North Atlantic sector, the NAM corresponds to a poleward shifted North Atlantic jet, whereas in

the North Pacific sector, the NAM corresponds to a weaker subtropical jet [*Ambaum et al.*, 2001; *Eichelberger and Hartmann*, 2007]. We will return to this point in Section 3.

While our observational analysis has so far focussed on monthly and longer timescales, the dynamics of zonal mean extratropical variability, and of the AMs in particular, is controlled to a large degree on shorter timescales, as we will discuss in Section 3. A daily index of the AM is found by projecting the AM EOF $\mathbf{e}_1$ (which is typically calculated, as we have, from seasonal mean or low pass filtered data) onto the daily circulation using $\mathbf{y}_{1,\text{daily}} = \mathbf{Z}_{\text{daily}}\mathbf{e}_1/\mathbf{e}_1^T\mathbf{e}_1$, where $\mathbf{Z}_{\text{daily}}$ represents the daily time series of the geopotential anomaly at the p spatial points of the EOF. When AM variability is analyzed on daily-to-multiple week timescales, the vertically coherent static patterns in Plates 3-4 resolve into vertically propagating signals in which tropospheric AM anomalies lag stratospheric AM anomalies by periods of several weeks [*Baldwin and Dunkerton*, 1999, 2001; *Baldwin and Thompson*, 2009]. This relationship is diagnosed by calculating the AM and its principal component time series at each vertical level and then using lag-correlation or compositing techniques to determine the vertical variation of the time lags. As an example, we show in the top panel of Plate 5 a *Baldwin and Dunkerton* [2001] type composite over low NAM index events (weak or warm stratospheric vortex events). The figure shows a vertically coherent NAM signal that propagates down from the stratosphere into the troposphere and leads to like-signed NAM anomalies in the troposphere that persist for 40 days or more. These downward propagating signals are typically associated with extreme events in the stratosphere, such as stratospheric sudden warmings and vortex intensification events [*Limpasuvan et al.*, 2004, 2005]. For example, during stratospheric sudden warmings, a weak vortex anomaly (negative NAM event) is found to burrow down into the stratosphere; the NAM signal then makes its way into the troposphere, where it is manifested as an equatorward shift of the storm tracks and an equatorward intensification of the tropospheric jet [*Baldwin and Dunkerton*, 2001]. The bottom panel of Plate 5 shows a similar calculation to the top panel, but using the geopotential averaged over the 60^0N-90^0N polar cap. The similarity between the two panels suggests that we can use the polar cap geopotential as a simple proxy for the AM; we will do so in Section 3.

The multiple week lag between stratospheric and tropospheric AM signals suggests that the stratosphere can provide a source of predictability that extends beyond the classical limit for tropospheric weather predictability [*Baldwin et al.*, 2003]. *Baldwin et al.* [2003] argue that the tropospheric AM is observed to be more persistent in winter and that this persistence results from stratosphere-troposphere coupling. A version of their analysis is presented in Plate 6, from *Gerber et al.* [2008a], which plots in the top row the seasonal cycle of the autocorrelation decay timescale of NAM and SAM variability from the NCEP reanalysis. The characteristic timescales of the AM, consistently with Plate 1, is on the order of 1-2 weeks in the troposphere and several weeks in the stratosphere, with a strong peak during the active season for the SAM and NAM, suggesting a stratospheric connection for tropospheric persistence of these modes [*Baldwin et al.*, 2003]. The bottom row of Plate 6 shows the same diagnostic for the set of climate simulations in the Intergovernmental Panel on Climate Change's Fourth Assessment Report, which we will comment on in Sections 3 and 4.

We conclude this section by discussing the regional, i.e. the longitudinal, structure of the AMs in the troposphere, which has been the subject of considerable debate [e.g. *Deser*, 2000; *Ambaum et al.*, 2001; *Wallace and Thompson*, 2002; *Vallis et al.*, 2004; *Kushner and Lee*, 2007]. If we regress the NAM index on a longitudinally varying field such as the two dimensional sea-level pressure, we typically obtain a pattern consisting of a low pressure anomaly over the pole and high pressure anomalies over the North Atlantic and North Pacific (see Figure 1a, from *Deser* [2000], which shows the regression of the sea-level pressure on the NAM index from *Thompson and Wallace* [1998]). The regressions have a predominantly zonally symmetric or "annular" appearance, although the amplitude of the patterns is greater over the oceans than over land. Similar predominantly zonally symmetric structures are found in both hemispheres whether or not the input to the EOF calculation [$\mathbf{X}$ in (1)] is zonally averaged [*Thompson and Wallace*, 2000; *Baldwin and Thompson*, 2009]. Thus, the zonal structure of the circulation that generates the AM is not critical to the zonal structure of the circulation that is coherent with the AM.

The point of debate about the zonal structure of the AMs centers on the fact that the zonal structure depends strongly on the analysis domain: for example, when the domain of the EOF calculation is restricted to the North Atlantic basin, the Pacific centre of action is no longer present in the regression and only the North Atlantic Oscillation type structure remains (Figure 1b); similarly when the domain is restricted to the North Pacific basin, only a North Pacific centre of action remains (Figure 1c). While all three patterns share a similar meridional structure, there is no coherence between the basins [*Deser*, 2000]. Consistently, on daily timescales it is found that high AM index

days are associated with regional (less than 90-degree scale) dipolar circulation anomalies [*Cash et al.*, 2002; *Vallis et al.*, 2004; *Kushner and Lee*, 2007]. This is in contrast to what we found for the vertical structure: for example the vertically coherent structures in Plate 3 involve only lower tropospheric information, and the vertically propagating stratosphere-troposphere signal in Plate 5 demonstrates a consistent statistical link between the zonal mean tropospheric and stratospheric circulation.

Kushner and Lee [2007] explore the connection between hemispheric AM variations and regional-scale variability. They find that day-to-day zonal-mean AM variability is consistent with the occurence of zonally localized dipolar patterns that have a decoherence width of about 90^0 longitude and that propagate eastward with a phase speed of about 8^0 longitude per day. In Figure 2, the regression pattern in surface circulation and the longitude-time propagation structure for these dipolar patterns in the Southern Hemisphere are plotted. *Kushner and Lee* argue that these patterns, which are similar in the Northern Hemisphere and Southern Hemisphere, are propagating versions of NAO type variability; outside the North Atlantic sector they are not dominant but secondary patterns of variability. These regression patterns have a westward phase tilt with height, suggesting that they are propagating and moderately baroclinic long waves. *Kushner and Lee* propose that these waves arise spontaneously and randomly, and their projection onto the zonal mean produces a zonal mean anomaly with the meridional structure of the zonal-mean AM. These ideas are not fully explored and have yet to be reconciled with the better established viewpoint that AM dynamics involves an interaction between synoptic eddies and the zonal mean flow. This viewpoint will be discussed in the next section.

3. ELEMENTARY IDEAS ON ANNULAR MODE DYNAMICS

If the AMs represent the dominant fluctuations of the extratropical zonal mean circulation, then *eddy mean flow interactions*, in which the zonal flow controls the eddies and the eddies exert a return control on the zonal mean flow, are required to explain AM dynamics. To see why, consider the role of eddies in classical quasigeostrophic (QG) dynamics [e.g. *Andrews et al.*, 1987]. For the QG scaling that the extratropical circulation is observed to satisfy, the zonal mean circulation evolves according to (see the Appendix)

$$\overline{q}_t + (\overline{v'q'})_y = \overline{S}. \qquad (4)$$

where coordinate subscripts represent partial derivatives, overbars represent the zonal mean, primes represent eddy (zonally asymmetric) quantities, v is the meridional geostrophic velocity, q is the QG potential vorticity, and S is a forcing and dissipation operator that includes the effects of momentum dissipation and diabatic heating. In this notation, $\overline{v'q'}$ represents the meridional flux of eddy potential vorticity. Consider how temporal anomalies in the zonal mean potential vorticity, which we denote, $\overline{q}^a$, are related to temporal anomalies in the zonal mean potential vorticity flux, $(\overline{v'q'})^a$. Using the principal of inversion of potential vorticity [*Hoskins et al.*, 1985], from the zonal mean potential vorticity anomaly $\overline{q}^a$ and related surface information we can diagnose the zonal mean geopotential anomaly, and hence the zonal mean wind anomaly from geostrophic balance and the zonal mean temperature anomaly from hydrostatic balance. Thus (4) represents the evolution of the entire zonal mean state.

If we remove the climatological mean from (4), multiply by $\overline{q}^a$, and take a density weighted volume average (denoted by angle brackets), we obtain a variance equation for the zonal mean potential vorticity anomaly:

$$\frac{d}{dt}\left\langle \frac{1}{2}(\overline{q}^a)^2 \right\rangle = -\left\langle (\overline{v'q'})^a_y \cdot \overline{q}^a \right\rangle + \left\langle \overline{S}^a \cdot \overline{q}^a \right\rangle, \qquad (5)$$

where $(\overline{v'q'})^a_y$ and $\overline{S}^a$ represent the eddy potential vorticity flux divergence anomaly and the dissipation anomaly. In the Appendix, we argue that $\left\langle \overline{S}^a \cdot \overline{q}^a \right\rangle \leq 0$ to within a boundary term of indeterminate sign. If this boundary term can be neglected, this implies that $\overline{S}^a$ acts to attenuate the amplitude of zonal mean potential vorticity anomalies. This in turn would mean that extratropical dynamics cannot sustain fluctuations of the zonal mean unless, averaged over the spatial domain, the eddy potential vorticity flux convergence anomaly $-(\overline{v'q'})^a_y$ is positively correlated with the potential vorticity anomaly $\overline{q}^a$. This suggests that AM dynamics requires the eddy potential vorticity flux anomalies to amplify rather than attenuate local potential vorticity anomalies, over some part of the domain, in order to maintain AM variability.[1] We will argue that the means by which AM variability is maintained by eddy forcing is distinct in the stratosphere and troposphere.

In Plate 5 we showed that the AM is represented well by the geopotential averaged over the polar cap; [*Baldwin and Thompson*, 2009] discuss the strengths and weaknesses of using the polar cap as a proxy for the AM. For dynamical purposes the polar cap is a useful control volume to work with. In the context of QG dynamics, following a similar approach to *Hu and Tung* [2002], we consider the integrated potential vorticity for

a polar cap bounded at the top and bottom by $z = z_T$ and $z = z_B$ and bounded meridionally by the North Pole $y = y_N$ (90^0N) and by $y = y_S$. This will lead to relationships between circulation, polar cap isentropic thickness, eddy fluxes, and dissipation. If we denote a density weighted average over this polar cap by $<>_p$, we find that the integrated potential vorticity anomaly tendency satisfies (see Appendix)

$$< \overline{q_t{}^a} >_p \;=\; \int_{z_B}^{z_T} dz\,(\rho_0 \overline{u_t{}^a})\Big|_{y=y_S} + \int_{y_S}^{y_N} dy\left(f_0\rho_0 \overline{\theta_t{}^a}/\theta_{0z}\right)\Big|_{z=z_B}^{z=z_T} \qquad (6)$$

Here, the $|_{y=y_S}$ notation represents the integral evaluated at $y = y_S$, and the $|_{z=z_B}^{z=z_T}$ notation represents the integral evaluated at $z = z_T$ minus the integral evaluated at $z = z_B$. Locally, the potential vorticity, which is approximated by the QG potential vorticity, represents the ratio of the absolute vorticity to the thickness between isentropic surfaces, or the product of the absolute vorticity and static stability. A positive potential vorticity tendency requires either (or both) a positive tendency in vorticity or a negative tendency in thickness (which is a positive tendency in static stability). Analogously, a positive polar-cap averaged potential vorticity tendency involves either (or both) a positive tendency in circulation around the polar cap (acceleration of the zonal wind $\overline{u}$ around the polar cap), as represented by the first term on the right hand side of (6); or a negative tendency in average thickness, as represented by an increase in the vertical difference of the term proportional to $\overline{\theta^a}$ on the right hand side of (6). These effects are coupled via the residual circulation that is extensively discussed in *Andrews et al.* [1987] and *Haynes et al.* [1991].

Polar cap potential vorticity anomalies can be induced by anomalies in eddy fluxes and in dissipation. We can express the QG potential vorticity flux in terms of the QG Eliassen Palm (E-P) flux:

$$\begin{aligned} \overline{v'q'} \;&=\; \rho_0^{-1}\left[-(\rho_0\overline{v'u'})_y + (\rho_0 f_0 \overline{v'\theta'}/\theta_{0z})_z\right] \\ &=\; \rho_0^{-1}\nabla\cdot\vec{F}, \end{aligned} \qquad (7)$$

where

$$\vec{F} \;=\; (F_{(y)}, F_{(z)}) \;=\; (-\rho_0\overline{v'u'}, \rho_0 f_0 \overline{v'\theta'}/\theta_{0z})$$

is the E-P flux. We find that

$$\begin{aligned} < \overline{q_t{}^a} >_p \;&=\; \int_{z_B}^{z_T} dz\rho_0(\overline{v'q'})^a\Big|_{y=y_S} + < \overline{S^a} >_p \\ &=\; \int_{z_B}^{z_T} dz\left(F^a_{(y)}\right)_y\Big|_{y=y_S} \\ &\quad + F^a_{(z)}\Big|_{z=z_B,y=y_S}^{z=z_T,y=y_S} + < \overline{S^a} >_p \end{aligned} \qquad (8)$$

The polar cap potential vorticity can thus be increased by an eddy flux of potential vorticity into the cap. This eddy potential vorticity flux can involve either (or both) eddy momentum flux convergence at the cap boundary, which is equivalent to a vorticity flux into the cap, since $F_{(y)} = (-\overline{u'v'})_y = \overline{v'\zeta'}$; or a transport of thickness (vertically varying meridional heat transport) into the meridional boundary of the cap, via the terms involving the vertical difference in $F_{(z)} \propto \overline{v'\theta'}$ which are evaluated only at the polar cap boundary. We note that the vertical EP flux at a given latitude drives potential vorticity anomalies poleward of that latitude. Through the EP flux divergence, both eddy thickness and momentum fluxes can thus induce a PV tendency, which corresponds to a tendency in circulation or in stratification. The connection of the vertical EP flux (meridional heat flux) to stresses on the mean flow is related to the concept of *form stress*, which involves the correlation between fluctuations in pressure and in the height of isentropic surfaces for a system in geostrophic and hydrostatic balance [e.g. *Vallis*, 2006].

We consider two special cases of the relationships in (8). If we take $z_B \to 0$, where $z = 0$ is the Earth's surface (expressed approximately in log-pressure coordinates) and $z_T \to \infty$, we obtain the well-known vertical mean momentum balance between acceleration, mechanical forcing, and eddy momentum fluxes (see Appendix):

$$\int_0^\infty dz\rho_0\left[\overline{u_t^a} + (\overline{u'v'})_y^a - \overline{X^a}\right] = 0 \text{ at } y = y_S, \qquad (9)$$

where X represents x-momentum dissipation. This expression provides a mechanism for eddy momentum fluxes to produce the dipolar wind anomalies that characterize the tropospheric AM. Eddy momentum flux divergence (or vorticity flux) out of one latitude band into another will be balanced by dipolar wind structures via either the $\overline{u}_t$ term or the X term. This description suggests that simple layer models that are dominated by vorticity fluxes will be useful to understand the vertically coherent AM dynamics. The vertical integral averages out the vertical coupling by the mean meridional circulation: when we look in more detail, we see that the eddy momentum transfer occurs mainly in the upper troposphere and is communicated vertically to the surface via a thermally indirect eddy driven mean meridional circulation, which is balanced by frictional dissipation [*Limpasuvan and Hartmann*, 2000]. The mean meridional circulation that is coherent with eddy momentum fluxes is clearly seen in AM regressions [*Thompson and Wallace*, 2000].

As another special case, it is observed that for the lower stratosphere the contribution from the meridional component of the E-P flux to the total eddy driving is small compared to the vertical

contribution [*Newman et al.*, 2001; *Hu and Tung*, 2002; *Polvani and Waugh*, 2004]. Thus, we expect stratospheric AM variability, which involves fluctuations in the strength of the polar vortex, to be dominated by variability in the vertical EP flux component and thus by the thickness flux. For example, on intraseasonal to interannual timescales, the vertical component of the EP flux correlates very well with polar cap stratospheric temperatures [*Newman et al.*, 2001; *Polvani and Waugh*, 2004]. This suggests that a useful simple model of the stratosphere will focus on the forcing of stratospheric winds by vertical EP fluxes.

Before discussing simple theoretical models, we return to observations to examine the eddy fluxes that are coherent with the AM. *Limpasuvan and Hartmann* [1999, 2000] calculate the contributions to $\vec{F}$ and $\nabla \cdot \vec{F}$ (in primitive equation form, which is approximated by (7)) that are coherent with the SAM and NAM index via a composite technique, using all-year data. The main focus of the paper is on the tropospheric AMs in observations and general circulation models. Plate 7 shows composite EP flux cross sections for high AM index conditions (top row), for low AM index conditions (middle row), and their difference (bottom row), adapted from *Limpasuvan and Hartmann* [2000]. There is some degree of hemispheric symmetry in these patterns. In both hemispheres, high AM index conditions correspond to a deflection of EP flux away from the poles and towards the tropics. This figure also shows similar behaviour in the stratosphere in both hemispheres: high AM index conditions correspond to positive EP flux divergence anomalies in the high latitude stratosphere of each hemisphere, indicating reduced wave driving in the high latitude stratosphere. The pattern of wave driving is consistent with the AM structure in the manner we just described: equatorward deflection of wave activity, since $F_{(y)} \propto -\overline{u'v'}$, corresponds to an increased poleward eddy flux of eastward momentum, which exerts a westward stress on the equatorward side and an eastward stress on the poleward side. This is consistent with the dipolar structure of the tropospheric wind anomaly (e.g. Plate 4). Reduced wave driving in the stratosphere allows polar stratospheric temperatures to relax closer to radiative equilibrium and hence allows the polar vortex to strengthen. A key difference between the two hemispheres is the relative importance of stationary versus transient eddies in the EP fluxes — stationary eddies are dominant in the eddy momentum flux driving in the Northern Hemisphere, while transient eddies dominate the eddy momentum flux driving in the Southern Hemisphere [*Limpasuvan and Hartmann*, 2000].

The balance between eddy fluxes, circulation anomalies, and dissipation does not address the fundamental questions of how the AMs arise, why they are the dominant mode of variability, what determines their evolution and dynamics, and what couples their stratospheric and tropospheric parts. Much insight can be gained by careful observational analysis. For example, *Lorenz and Hartmann* [2001, 2003] investigate the role of the interactions between eddy momentum fluxes and the AM zonal mean wind anomalies in detail and quantify the positive feedback between the two. In this feedback, the zonal mean flow organizes the eddies in such a way as to enhance the momentum flux driving of the AM, and hence its persistence. But to answer our fundamental questions it is also important to consider simplified theoretical models within a model hierarchy [*Held*, 2005]. We first consider the tropospheric AM, which, as we learned from our observational analysis, is not critically dependent on coupling to the stratosphere (see the discussion of Plate 3), and for which vorticity fluxes associated with horizontal propagation of EP flux will play a prominent role. For the stratospheric AM, we will turn to models in which the dominant eddy driving comes from form stresses associated with the meridional eddy flux of heat; for these models, vertical propagation of EP flux dominates.

Fundamentally, variability in the extratropical tropospheric zonal mean circulation reflects eddy mean-flow interactions involving baroclinic and stationary eddies; these give rise to considerable variability even with time independent boundary conditions [e.g. *Robinson*, 1991]. Coupling to the ocean, to the land surface, to the stratosphere, etc., might modulate this dynamics but does not exert a leading order control. For example, one of *Limpasuvan and Hartmann*'s [2000] main conclusions is that an atmospheric general circulation model (AGCM) with a prescribed sea surface temperatures (SST) field that varies seasonally, but not from year to year, produces a realistic NAM and SAM structure with eddy fluxes that closely resemble the features seen in Plates 4 and 7. This also holds true for coupled ocean atmosphere GCMs in which SSTs are predicted, confirming that coupling to the ocean is not a critical issue for AM variability [*Miller et al.*, 2006]. An important caveat, which we will return to in Section 4, is that these GCMs produce AMs that are too persistent. This is evident from the bias towards the long timescales for the climate model simulations seen in the bottom row of Plate 6 [adapted from *Gerber et al.*, 2008a]. AM variability appears in AGCMs with simplified boundary conditions (such as an aquaplanet) [*Cash et al.*, 2002] and in *simplified GCMs*, which will be discussed in Section 4.1, with linear representations of diabatic

heating and mechanical dissipation [*Yu and Hartmann*, 1993; *Held and Suarez*, 1994; *Polvani and Kushner*, 2002; *Song and Robinson*, 2004; *Gerber and Polvani*, 2009; *Ring and Plumb*, 2008]. But an AGCM, in any configuration, still represents a highly complex system, and it is useful to have in hand even simpler models with which to test ideas.

The simplest model in which realistic tropospheric AM variability is spontaneously generated is a two-layer QG model with the density relaxed to a prescribed baroclinically unstable reference distribution. The width of the region over which this reference distribution is baroclinically unstable determines the width of the baroclinic zone. In one limit the baroclinic zone is infinitely wide and zonal mean variability consists of multiple jets that exhibit a slow and unpredictable meridional wander [e.g. *Panetta*, 1993]; the jet and eddy scales are internally determined by differential rotation (β) and the eddy energy, which is related to the imposed baroclinicity. *Lee and Feldstein* [1996] show that the emergence of more realistic AM type variability — which they describe in terms of zonal index variability — is linked to the width of the baroclinic zone. Some of the possible regimes are seen in Figure 3: when the jet is narrow (Figure 3a) the leading mode is a monopolar "pulsing" mode and represents an alternate sharpening and flattening of the jet profile. As the jet widens (Figure 3b), a dipolar AM EOF emerges that corresponds to a meridionally shifting jet. Once the baroclinic zone is sufficiently wide, a double jet structure emerges and the leading EOF represents the degree to which the two jets are merged together or separated (Figure 3c). Finally, for an even wider zone, the leading mode involves AM dipoles for both jets (Figure 3d). In all these regimes the zonal index or AM EOF is present, but it is not always the dominant mode [see also *Feldstein*, 2000].

An arguably even simpler model of tropospheric AM variability is the stirred barotropic model of *Vallis et al.* [2004], in which the forcing from baroclinic eddies is not internally generated but is externally imposed as a stochastic forcing. The nonlinear barotropic potential vorticity dynamics organizes this forcing into a jet whose variability can be tuned by adjusting the structure of the forcing. Similarly to *Lee and Feldstein* [1996], the transition from a narrow-jet "pulsing" regime to a wide-jet "wobbling" regime is governed by the width of the stirring region (Figure 4). This model can also be used to investigate the effect of storm-track localization on the formation of the North Atlantic Oscilation, thus linking in a simple framework the transition from hemispheric-scale to regional-scale variability. *Gerber and Vallis* [2005] strip the dynamics down even further by studying AMs using stochastic models in which angular momentum conservation is built in as a global meridional constraint and coupling in longitude can be introduced in a controlled way.

We return to the observation in Section 2 that the NAM and SAM are more similar to each other in the troposphere than the Northern and Southern Hemisphere tropospheric jets. Classically, the observed zonal mean zonal wind reflects two types of jets: the *subtropical jet* for which axisymmetric angular momentum transport from the tropics are important, and the higher latitude *eddy-driven jet* which is dominated by eddy mean-flow interactions we have just described [e.g. *Lee and Kim*, 2003]. (This classical viewpoint is evolving with the realization that eddy potential vorticity fluxes are also important for the subtropical jet [e.g. *Kim and Lee*, 2001; *Walker and Schneider*, 2009].) The Southern Hemisphere November troposphere zonal wind displays aspects of both jets: there is an upper tropospheric (baroclinic) subtropical jet core near 30^0S in the upper troposphere and a vertically deep (equivalent barotropic) eddy-driven jet near 50^0S (bottom row, left panel of Plate 4). The SAM corresponds to meridional shifts of the latter feature. In the Northern Hemisphere, by contrast, the zonal mean jet in JFM (bottom row, middle panel of Plate 4) is dominated by the subtropical jet near 30^0N. But for the tropospheric zonal mean wind sector averaged over the North Atlantic region (not shown), a higher latitude eddy driven jet is seen and the NAM corresponds to poleward and equatorward shifts of this feature [*Ambaum et al.*, 2001; *Eichelberger and Hartmann*, 2007]. Thus, a similar connection between the eddy driven jet and the AM can be found in both hemispheres, although the connection is more regional in the Northern Hemisphere. *Eichelberger and Hartmann* [2007] use a simplified GCM (Section 4) to explain dynamically the local relationships between Northern Hemisphere jet structure and NAM variability.

Unlike the tropospheric AM, which is manifested as a jet meander, the stratospheric AM is manifested as a strengthening and weakening of the jet. Eddy forcing is important in stratospheric AM variability but stratospheric waves are primarily generated from tropospheric sources that are external to the stratosphere. The model of *Holton and Mass* [1976] that has been further explored and developed by many researchers [e.g. *Yoden*, 1987; *Plumb and Semeniuk*, 2003; *Scott and Polvani*, 2006] provides the simplest formulation for capturing stratospheric AM variability. In this model, the zonal mean stratospheric circulation is relaxed towards a prescribed radiative equilibrium profile. Planetary Rossby waves are generated by prescribing a zonally asymmetric lower boundary, conventionally chosen to represent the stationary wave

field in the upper troposphere. The upwelling wave activity flux can be calculated in various ways; in the simplest formulation it is parameterized using WKB theory. In Figure 5, from *Plumb and Semeniuk* [2003], the wind and geopotential variability resembles the observed downward propagating AM signals in the stratosphere. The model in *Plumb and Semeniuk* [2003] is effectively one dimensional in the vertical and represents in a simple way the interaction between stationary Rossby waves with upward group velocity and the zonal mean flow. The resulting downward propagating signal in geopotential and winds is a consequence of enhanced wave activity absorption (EP flux convergence) where the winds are weaker, and the reestablishment of the eastward winds at levels shielded from upward propagating wave activity.

The Holton-Mass model exhibits distinct circulation regimes that depend mainly on the amplitude of the zonally asymmetric lower boundary forcing. For example, in the weakly forced subcritical regime that was explored in *Plumb and Semeniuk* [2003] and is illustrated in Figure 5, the period and evolution of the stratospheric flow is determined entirely by the zonally asymmetric forcing of the lower boundary. *Plumb and Semeniuk* [2003] show that downward propagation of $\overline{Z^a}$ does not imply downward propagation of stratospheric information, since the source of the wave driving and the wave activity absorption are determined from the prescribed boundary evolution and state information below a given level. This example shows how some aspects of stratospheric variability might be largely determined by tropospheric dynamics. In the strongly forced supercritical regime [e.g *Yoden*, 1987; *Scott and Polvani*, 2006], the zonal mean Holton-Mass model exhibits spontaneous vacillations of the zonal wind even for time independent lower boundary forcing. This regime provides an example of a more active stratosphere that might not depend on the detailed time evolving state of the troposphere, provided that the overall wave forcing from the troposphere is sufficiently strong. Thus within this simple model we see a wide range of possibilities for the way in which the stratosphere might depend on the troposphere.

To summarize, we have learned that tropospheric and stratospheric AM variability can be isolated in truncated models whose dynamics are complementary. Tropospheric AM models require relatively fine horizontal resolution to capture the synoptic scale eddies that are involved in eddy momentum flux transport, but require only coarse vertical resolution involving even only one or two vertical layers. Stratospheric AM models require relatively fine vertical resolution to capture the downward propagating wave activity absorption region, but require only coarse horizontal resolution to capture planetary Rossby waves. But neither type of simple model can realistically simulate the observed coupling, via the AMs, between the troposphere and stratosphere that is depicted in Plate 5. One might imagine constructing a model that couples the two types of truncated systems, but this direction has not been explored to our knowledge. To simulate realistic AM variability, we turn in the next section to more realistic GCMs with sufficient vertical and horizontal resolution to capture the dynamics as a whole.

4. ANNULAR MODES IN GENERAL CIRCULATION MODELS

Given the limitations of the truncated models discussed in Section 3, we turn to models of greater complexity in the model hierarchy, and consider the simulation of AM variability and AM responses to climate forcings in simplified GCMs and comprehensive climate models. We will also discuss recently developed ideas related to the fluctuation dissipation theorem, whose application to climate simulation helps elucidate the simulated AM response to climate forcings. Along the way, we will consider the general question of *stratospheric influence* on the troposphere, in which the AMs are strongly implicated.

4.1. Simulation of Intraseasonal Variability

As discussed in Section 3 modern climate models generally simulate the AM spatial structure credibly, especially in the troposphere [*Limpasuvan and Hartmann*, 2000; *Miller et al.*, 2006]. Indeed, realistic tropospheric AM structures appear to be a basic feature of any model that realistically represents the zonal mean circulation and tropospheric large-scale waves (baroclinic and stationary waves). It was also established soon after the original work of *Baldwin and Dunkerton* [1999, 2001] that comprehensive GCMs with sufficient stratospheric resolution are capable of capturing intraseasonal stratosphere-troposphere coupling in free-running climate [e.g. *Christiansen*, 2001] and seasonal forecast [e.g. *Charlton et al.*, 2004] settings. *Christiansen*'s [2001] simulations of a free running climate model (with no information about the observed atmospheric state) are able to spontaneously produce realistic downward propagating NAM anomalies that progress from the stratosphere into the troposphere. In current models with good stratospheric representation [e.g. *Baldwin et al.*, 2010], downward propagating stratosphere-troposphere signals appear to be a generic feature that is easy to capture in some form.

Charlton et al. [2004] demonstrate a practical application of this capability by using a numerical weather prediction model to investigate whether stratospheric information can provide useful predictive information in the troposphere beyond the limit of deterministic weather prediction. They initialize ensembles of simulations with different polar vortex strengths and obtain a downward propagating NAM response which penetrates into the troposphere over the course of several weeks (see Figure 6). Practically, this study shows that accurate stratospheric information and representation can potentially improve seasonal forecasts. The question of stratospheric representation on capturing tropospheric AM variability arises in a variety of contexts, including the response to stratospheric sudden warmings, ENSO-related variability, and to variability in seasonal snow cover [e.g. *Gong et al.*, 2002; *Scaife and Knight*, 2008; *Fletcher et al.*, 2009; *Ineson and Scaife*, 2009; *Bell et al.*, 2009; *Cagnazzo and Manzini*, 2009]. But these studies, and similar ones which examine the downward influence of altered stratospheric initial states [e.g. *Hardiman and Haynes*, 2008], do not unambiguously address the question of whether the stratosphere exerts a downward influence on the troposphere. This is because the prescribed stratospheric state might depend on the prior state of the troposphere, in particular the history of wave activity fluxes from the troposphere to the stratosphere [*Plumb and Semeniuk*, 2003; *Polvani and Waugh*, 2004; *Scott and Polvani*, 2006]. We will show a more direct example of stratospheric influence in connection with climate responses to stratospheric cooling and ozone depletion below.

Having established that comprehensive climate models capture the downward propagating AM signals, the dynamical question of what the minimum ingredients are to capture these signals remains open. To answer this, we turn to "simplified GCMs", by which we mean models that integrate the primitive fluid equations of motion on the sphere at relatively fine horizontal and vertical resolution but that include only the simplest representations of radiative transfer and subgrid scale momentum dissipation, and that do not include moisture [e.g. *Scinocca and Haynes*, 1997; *Polvani and Kushner*, 2002; *Taguchi and Yoden*, 2002; *Gerber and Polvani*, 2009]. Simplified GCMs typically represent diabatic heating by a term $-(T - T_{eq})/\tau_r$ in the thermodynamic equation, which corresponds to Newtonian relaxation to a prescribed equilibrium temperature profile T_{eq} on a radiative timescale τ_r; and represent momentum dissipation by a simple mechanical drag $-\vec{u}/\tau_d$, where $\vec{u}$ is the horizontal velocity and τ_d is a timescale for momentum dissipation. The reference temperature profile T_{eq} is baroclinically unstable in the troposphere and leads to an eddy-driven jet stream qualitatively similar to observed. In the stratosphere, T_{eq} is constructed to produce a polar night jet. We emphasize that these models are only *relatively* simple compared to comprehensive GCMs; in absolute terms, they represent a highly complex dynamical system of partial differential equations. Still, compared to comprehensive GCMs, they have the advantage of being relatively easy to reproduce in a manner that allows them to provide the basis for benchmark calculations across different research groups [*Held and Suarez*, 1994; *Galewsky et al.*, 2004].

In simplified GCMs, stratospheric variability depends in a complicated way on tropospheric boundary conditions and dynamics. For example, models with time independent and zonally symmetric boundary conditions can generate some realistic aspects of stratospheric variablity [*Scinocca and Haynes*, 1997], and the stratospheric mean state and variability are sensitive to changes in topographic amplitude and structure [*Taguchi and Yoden*, 2002; *Gerber and Polvani*, 2009]. By simply varying the topographic forcing, these models can be tuned to represent the stratospheric variability of either hemisphere [*Taguchi and Yoden*, 2002].

Our interest in this subsection is to determine the minimum requirements for generating the downward propagating AM signals. *Gerber and Polvani* [2009] addressed this question by varying topographic scale and amplitude. For a given time independent T_{eq} they are able to tune their model from a stronger polar vortex regime without topography in which the AMs are tropospherically trapped, to a weaker polar vortex regime with topography in which the AMs have large amplitude in both the troposphere and stratosphere (Plate 8). In this regime, the model is capable of producing realistic coupled stratosphere-troposphere events (Plate 9a), including the build up of wave activity flux into the stratosphere that precedes a negative stratospheric NAM event (Plate 9b). This regime is very sensitive: if the topographic amplitude is increased, the vortex becomes relatively weak and only produces small amplitude NAM events; if the topographic amplitude is reduced, the vortex becomes too strong and robust to be significantly weakened by wave activity pulses; if the wavenumber of the topography is changed, the character of the variability of the polar vortex also changes qualitatively. As for the other examples we will describe in this section, none of these sensitivities were predicted by preceding theoretical work, which highlights how simplified GCMs remain a primary theoretical tool to explore coupled stratosphere-troposphere variability.

To conclude this subsection on intraseasonal AM variability, we consider the tropospheric ori-

gin of stratospheric NAM anomalies in connection with surface forcing, including forcing from El Niño-Southern Oscillation (ENSO) related sea surface temperatures in the tropical Pacific [*Ineson and Scaife*, 2009; *Bell et al.*, 2009; *Cagnazzo and Manzini*, 2009; *Garfinkel and Hartmann*, 2008] and from snow cover anomalies over Eurasia [e.g. *Cohen and Entekhabi*, 1999; *Gong et al.*, 2002; *Cohen et al.*, 2007; *Fletcher et al.*, 2009]. Although the stratosphere is capable of generating internal vacillations independently of the state of the troposphere, as discussed in Section 3, it is likely that some portion of stratospheric variability should potentially originate from tropospheric variability. Recent work by *Garfinkel et al.* [2010] shows that this should occur, for ENSO and for Eurasian snow forcing, when the wave component of circulation anomalies related to the surface forcing align with the climatological stationary wave and thereby reinforce or attenuate the wave activity flux into the stratosphere. The lagged nature of the response implies that surface forcing can further extend the window of seasonal predictability via stratosphere-troposphere interactions. ENSO forcing provides a Rossby wave source from the tropics to the extratropics, and the work by *Ineson and Scaife* [2009] and *Cagnazzo and Manzini* [2009] shows that stratospheric representation makes a difference to how this wave activity drives zonal mean NAM anomalies. Surface forcing by Eurasian snow cover anomalies in fall can similarly enhance the tropospheric wave activity flux into the stratosphere, thereby inducing a dynamical warming and a downward propagating NAM signal in Northern Hemisphere winter. This variability is simulated in comprehensive GCMs in which the snow cover forcing is prescribed [*Gong et al.*, 2002]. The effect is sensitive to stratospheric details [*Fletcher et al.*, 2009] and is not captured as an intrinsic mode of variability in the CMIP3/IPCCAR4 models [*Hardiman et al.*, 2008]. This work suggests that obtaining improved predictability of AM events of this kind will require considerable improvements in the simulation of stationary waves and land-surface processes.

4.2. AM Climate Trends and Climate Responses

Much of the original interest in the AMs stemmed from the fact that circulation trends through to the end of the 20th century projected strongly onto the AMs, in a manner corresponding to a positive NAM trend in the Northern Hemisphere and a positive SAM trend in the Southern Hemisphere [*Thompson and Wallace*, 1998; *Thompson et al.*, 2000; *Hartmann et al.*, 2000; *Thompson and Solomon*, 2002]. For example, *Thompson et al.* [2000] show that the pattern of land-surface temperature trends in the Northern Hemisphere in the late 20th century are largely consistent with a positive NAM trend. In the Southern Hemisphere, *Thompson and Solomon* [2002] reported that the seasonality and pattern of SAM trends suggested a direct influence by ozone depletion on the tropospheric circulation of the Southern Hemisphere (see Figure 7a-b, from **?**). Since the NAM's peak in the late 1990's, the NAM trend has weakened and reversed [*Overland and Wang*, 2005; *Cohen and Barlow*, 2005], but the long term SAM trend remains robust [*Fogt et al.*, 2009]. Although current trends in the AMs are relatively ambiguous, understanding the cause and expected future of these trends remains a compelling research question. In this subsection, we will investigate AM responses to climate change in simplified and comprehensive GCMs, and in Subsection 4.3 highlight some theoretical issues related to these responses.

To see how circulation trends might relate to AM variability, suppose that a circulation related field like sea-level pressure exhibits a long-term trend. In the notation of Section 2, we can express a data matrix $\tilde{\mathbf{F}}$ of n observations at p spatial points, which has zero time mean at each point, as the sum of a linear trend term and a residual term:

$$\tilde{\mathbf{F}} = \mathbf{t}\mathbf{f}_\Delta^T + \mathbf{R}, \tag{10}$$

where $\mathbf{t}$ is an n-point column of times of observation and $\mathbf{R}$ is a residual term which has no linear trend. The spatial vector $\mathbf{f}_\Delta$ is a p-point column of trend coefficients, obtained by linear regression. (Alternatively, $\mathbf{f}_\Delta$ can represent simply the difference in the field between two time periods, e.g. 21st and 20th centuries, in which case no linear regression is carried out.) We are interested in what determines the spatial structure of this quantity and whether it is related to natural patterns of variability. For example, its projection on the AM is $\mathbf{f}_{\Delta,1} = {\mathbf{f}_\Delta}^T\mathbf{f}_1/\mathbf{f}_1^T\mathbf{f}_1$, where $\mathbf{f}_1 = \tilde{\mathbf{F}}^T\mathbf{y}_1/\mathbf{y}_1^T\mathbf{y}_1$ is the projection of the data matrix onto the PC time series of the AM. The projection coefficient $\mathbf{f}_{\Delta,1}$ provides the sign and degree of coherence between the trend pattern and the AM pattern; the quantity $\left({\mathbf{f}_{\Delta,1}}^T\mathbf{f}_{\Delta,1}\right) / \left({\mathbf{f}_\Delta}^T\mathbf{f}_\Delta\right)$ represents the fraction of variance represented by the AM-related component of the trend.

Figure 8, from *Miller et al.* [2006], shows the fraction of variance represented by the projection of the SLP response to climate change, diagnosed as the difference between the late 21st century and the early 20th century, onto the AM and other leading modes of extratropical variability, in the simulations included in the Coupled Model Intercomparison Project 3 prepared for the Intergovernmental Panel on Climate Change Report 4

(CMIP3/IPCC AR4). "Climate change" here includes the effects of anthropogenic greenhouse gas loading, ozone depleting substances like chlorofluorocarbons implicated in photochemical ozone loss, and aerosol polution. In the Southern Hemisphere, the figure shows that the SAM is the dominant pattern of SLP response, and *Miller et al.* [2006] show that the models produce a positive SAM response that agrees at least in sign with current trends. In the Northern Hemisphere the situation is much more complicated: the projection onto the NAM is weak, and *Miller et al.* [2006] show that there is disagreement on the sign of the projection onto the NAM as well. The situations in the two hemispheres are sufficiently different that they should be considered separately.

The most robust and well characterized AM response to climate forcing occurs in the Southern Hemisphere. In particular, there is now extensive evidence from observations and models that photochemical Antarctic ozone loss has induced a strong positive tropospheric SAM response. This is borne out in several studies involving comprehensive GCMs [e.g. *Sexton*, 2001; *Gillett and Thompson*, 2003; *Miller et al.*, 2006; *Cai and Cowan*, 2007; *Son et al.*, 2008; *Shaw et al.*, 2009]. The middle and bottom rows of Figure 7, from **?**, illustrate this effect: they show the Antarctic temperature and geopotential response for the CMIP3/IPCC AR4 models that include ozone depletion and those that do not. Models with ozone depletion consistently obtain a response in temperature and geopotential qualitatively similar to the observed trends, while those models without ozone depletion do not capture this response. Although this is not a clean comparison, because the sets of models represented in each row of Figure 7 are different, the main conclusion that ozone depletion is required to explain tropospheric circulation trends in the Southern Hemisphere in the late 20th century has been confirmed in several studies. The seasonal cycle of the response to ozone forcing is a downward propagating signal reminiscent of transient intraseasonal variability, and suggests a strong connection between the two; this might be expected from the perspective of fluctuation dissipation theory discussed in the next subsection, which connects internal modes of variability to climate responses. The effects on the troposphere of ozone depletion are expected to reverse as ozone depleting substance emissions are reduced and the ozone layer recovers into the mid 21st century [*Son et al.*, 2008; *Perlwitz et al.*, 2008]. This negative SAM response is expected to be accompanied by an equatorward shift of the tropospheric jet in Southern Hemisphere summer.

In simplified GCMs, the ozone-depletion effect on the tropospheric annular mode can be modelled by examining the stratosphere-troposphere response to cooling imposed in the stratosphere [*Polvani and Kushner*, 2002; *Kushner and Polvani*, 2004; *Gerber and Polvani*, 2009; *Chan and Plumb*, 2009]. *Polvani and Kushner* [2002]; *Kushner and Polvani* [2004] carry out such a simulation using a simplified GCM with zonally symmetric boundary conditions. In the simplified GCM, for sufficiently strong stratospheric cooling a dramatic poleward shift in the tropospheric jet occurs that is manifested as a positive tropospheric AM response that is consistent in sign with the effects of ozone depletion. These papers provide an unambiguous example of stratospheric influence on the tropospheric circulation in a simplified dynamical setting. As was the case for using simplified GCMs to understand intraseasonal variability, the models also provide dynamical insight. These and subsequent studies using simplified GCMs with various thermal and mechanical forcings [*Song and Robinson*, 2004; *Ring and Plumb*, 2007, 2008; *Chan and Plumb*, 2009] suggest that the same eddy mean-flow interactions that generate AM variability are also responsible for amplifying the response to imposed stratospheric forcing.

The simplified GCMs are sufficiently computationally inexpensive that wide parameter regimes can be explored. Such explorations show that many potential sensitivities exist that can generate non-robust responses to stratospheric cooling. The situation is nicely captured in Figure 9 [from *Chan and Plumb*, 2009], which shows that the strength of the poleward shift of the tropospheric jet (the positive SAM change) in response to stratospheric cooling (a strengthening polar vortex) is contingent on the existence of multiple regime behaviour for the tropospheric jet. When the tropospheric equator to pole temperature gradient is weak (in the first three columns of the figure), the tropospheric jet can be found in a subtropical position or can be in a state where it jumps between subtropical and extratropical positions on a very long timescale. Under these conditions, as the stratospheric polar vortex is strengthened (proceeding down the rows in the figure), the tropospheric jet position can be shifted poleward. This behaviour characterizes the regime found in *Polvani and Kushner* [2002]; *Kushner and Polvani* [2004]. As the tropospheric equator-to-pole temperature gradient is strengthened, the subtropical jet regime vanishes, and the sensitivity to stratospheric cooling is greatly reduced. Along the same lines, the tropospheric AM response to stratospheric cooling is greatly attenuated by the presence of zonal asymmetries [*Gerber and Polvani*, 2009]. Thus we see a connection between AM responses to climate perturbations and the ease with which the tropospheric jet can fluctuate between different regimes. The implications

of this behavior for present day, future, and past climates, has yet to be explored.

4.3. Perspective from Fluctuation Dissipation Theory

Why should we expect climate trends to be related to the AMs at all? The idea comes from a series of papers that have appealed to *fluctuation dissipation theory* in statistical mechanics [*Leith*, 1975; *Palmer*, 1999; *Gritsun and Branstator*, 2007; *Ring and Plumb*, 2008]. The theory postulates that, under general conditions, the principal pattern of response to climate forcings will project strongly onto persistent modes of internal variability of the system whose spatial structure is similar to that of the forcing. This means that many aspects of the response to climate change can be predicted from knowledge of the system's unforced climate variability. Formal techniques for diagnosing fluctuation-dissipation are described in *Ring and Plumb* [2008] and *Gritsun and Branstator* [2007]. Even without the formal approach, we can obtain useful information by empirically decomposing a response pattern into parts coherent with and unrelated to the internal variability [*Thompson et al.*, 2000; *Kushner et al.*, 2001; *Deser et al.*, 2004]. For example, if we consider the Southern Hemisphere response to greenhouse forcing [*Kushner et al.*, 2001], we can decompose the zonal wind response and the eddy momentum flux convergence response (Figure 10, top row) into a part that is coherent with the SAM (middle row) and a residual (bottom row). The residual is interpreted as the *direct* response to climate change, while the eddy driven AM response is interpreted as the *indirect* response. *Deser et al.*'s [2004] analysis of the Northern Hemisphere circulation response to high-latitude surface forcing used this approach to show that the direct response to sea ice and sea-surface temperature forcing in a GCM is localized to the forcing region, and that the indirect response is an eddy driven hemispheric teleconnection pattern. In a more controlled setting, *Ring and Plumb* [2007] show explicitly how the coherence of an applied forcing — in this case, a zonally symmetric momentum forcing applied in the vicinity of the jet in a simplified GCM — with the AM determines the sign and strength of the AM response.

Decomposing circulation responses into direct and indirect parts is useful for a broad brush characterization but is qualitative and has little predictive value. More quantitative analyses based on fluctuation-dissipation theory have been carried out in simplified GCMs [e.g. *Ring and Plumb*, 2008; *Gerber et al.*, 2008b] or in very long runs of comprehensive GCMs [e.g. *Gritsun and Branstator*, 2007, which deals with the global response to tropical heating]. A key prediction of the theory is that the expected pattern of response $\mathbf{f}_\Delta \sim \sum_i R_i \mathbf{f}_i \tau_i$, where R_i is the projection of the forcing onto mode $\mathbf{f}_i$ and τ_i is the decorrelation timescale of the unforced mode. Thus, we expect that more persistent modes will dominate the response, other factors being equal. Pursuing this idea, *Gerber et al.* [2008b] emphasize how AM timescales determine the amplitude of the response to external forcings: models with long AM timescales have an AM response that is proportionately greater, in agreement with the predictions of the theory. *Ring and Plumb* [2008] used fluctuation dissipation theory in even more detail in a simplified GCM forced mechanically and thermally. The responses in these simulations scaled linearly with the projection of the forcing onto the internal modes in general agreement with the theory, but the results did not agree quantitatively with its predictions.

There is thus fairly strong evidence to support the conclusion from fluctuation dissipation theory that the AM timescale is a key parameter controlling the strength of the indirect or free response to climate forcings. But the AM timescale, from the current modelling evidence, turns out to be highly non-robust and difficult to simulate accurately. For example, *Gerber et al.* [2008b] show that AM timescales in simplified GCMs are highly sensitive to horizontal resolution, vertical resolution, numerical diffusion, and other factors. In comprehensive GCMs, the IPCC AR4 models produce AM timescales that are too long in both the Northern Hemisphere and Southern Hemisphere, as seen in Plate 6. In simplified GCMs, we have already seen how some aspects of the sensitivity of the AM timescales is related to the structure of the jets; in particular, the existence of multiple regimes for the jet, in which the jet remains in a subtropical or in an extratropical location for long periods of time, greatly lengthens the timescale [*Chan and Plumb*, 2009]. In the IPCC AR4 models, *Kidston and Gerber* [2010] find a connection, similar to Chan and Plumb in the simplified GCMs, between the climatological bias, the AM timescale, and climate responses: those models with an equatorward bias in the Southern Hemisphere jet have a more persistent SAM and shift poleward more under climate change. From the analysis of simplified and comprehensive GCMs, in light of fluctuation dissipation theory, we conclude that AM responses might be too strong in present day GCMs. In addition, we conclude that the responses will be sensitive to many factors, even if the spatial structure and amplitude of the AMs are realistically represented in the models.

4.4. Stratospheric Representation and AM Responses

With this background we are in a better position to address the question of stratospheric influence on the AM response to tropospheric climate change. The seminal paper in this area is the study of *Shindell et al.* [1999], who argue that accurate stratospheric representation is necessary to reproduce the NAM trend of the late 20th century. The argument involves a comparison between two versions of comprehensive GCMs forced by anthropogenic greenhouse gas loading: a GCM with very few levels in the stratosphere (which we will call "low top"), and a model with a relatively more stratospheric resolution ("high top"). Of the two models, only the high-top model produces a positive NAM response similar to the observed trend. *Shindell et al.* argue that the only in the high-top model is the effect of planetary wave refraction properly accounted for: the positive NAM response in the stratosphere involves refraction of wave activity away from the polar lower stratosphere into low latitudes [*Shindell et al.*, 1999, 2001]. This work emphasizes that if the climate response truly projects onto the coupled stratosphere-troposphere AM then the wave driving response is intrinsic to the AM response and must be properly represented. While subsequent work has debated the findings and interpretation of the *Shindell et al.* work, it remains highly significant for the subsequent investigation it has stimulated.

The idea that stratospheric representation is important to tropospheric climate dates back to the work of Boville [*Boville*, 1984; *Boville and Cheng*, 1988]. This work shows that the configuration of the model stratosphere (including factors influencing the polar night jet like stratospheric diffusion, mechanical drag, and vertical resolution) has a significant influence on the tropospheric circulation. The patterns of sensitivity to stratospheric representation, in both the winds and the wave driving, resemble the AM structures. But the extension of this idea, that stratospheric representation is important to tropospheric climate change, is not currently straightforward to resolve. In apparent contradiction to *Shindell et al.* [1999], it is clear that low-top models are capable of obtaining AM responses similar to the observed trends [*Fyfe et al.*, 1999; *Kushner et al.*, 2001; *Miller et al.*, 2006]. But several factors confound simple generalizations: as we have said, the model responses are not robust (Figure 8); such responses might be exaggerated because of the long AM-timescale bias; and some observed AM trends are not robust. Thus, the issue of stratospheric representation on the response to climate change needs to be addressed separately for each climate response and for each model.

A necessary step to address the issue of stratospheric representation is to systematically vary stratospheric resolution while minimizing other changes. When model lid height is lowered and other changes are minimized, at least two models show relatively little sensitivity in their AM responses to climate forcing [*Gillett et al.*, 2002; *Sigmond et al.*, 2008; *Shaw et al.*, 2009]. For example, in *Sigmond et al.* [2008] and *Shaw et al.* [2009], a specialized low-top version of a high-top GCM (the Canadian Middle Atmosphere Model) is constructed so as to minimize inconsistencies between the two. (Plate 10 summarizes some of the results from these studies.) The lid of the low-top GCM is located at 10 hPa, which is lower than the lid of most present-day climate models. Yet both the low- and high-top models exhibit a strong positive NAM response to greenhouse warming [*Sigmond et al.*, 2008] and a strong positive SAM response to ozone depletion [*Shaw et al.*, 2009] — see Plate 10. Thus, stratospheric resolution by itself is not a key factor in controlling the AM response to climate forcings, at least in this model.

While in clean tests, stratospheric resolution does not necessarily influence tropospheric AM responses, the responses can be surprisingly sensitive to other factors. In particular, the models in Plate 10 are sensitive to the details of the parameterization of momentum dissipation by subgrid-scale gravity waves. In *Shaw et al.* [2009], for example, if the flux of momentum from parameterized "non-orographic" gravity waves is not deposited in the top model level in a manner that satisfies momentum conservation in the vertical, but instead allowed to figuratively "escape to space", the tropospheric SAM response to ozone depletion is supressed. In *Sigmond et al.* [2008], the positive tropospheric NAM response to greenhouse warming can be suppressed by increasing the strength of the orographic gravity wave flux from below. These sensitivities are relevant to current modelling practice, in which an escape-to-space boundary condition on the gravity wave fluxes near the model lid is often used, and in which a range of tunings of the orographic gravity wave flux are used. It would be interesting to see how much of the spread in AM responses in current GCMs could be attributed to inconsistencies in the implementation of gravity wave parameterizations, since these schemes are becoming better constrained observationally and better characterized numerically [*Alexander et al.*, 2009; *McLandress and Scinocca*, 2005].

5. CONCLUSION

The identification and characterization of the AMs, due in large part to the University of Washington 'school' with its hallmark of dynamically motivated observational analysis, has represented a significant advance in atmospheric science that has strengthened the link between our field and the environmental sciences as a whole. This is because the AMs provide a unifying framework for large-scale variability in the extratropics that links stratospheric and tropospheric dynamics, that highlights common strands between Northern and Southern Hemisphere variability, and that connects intraseasonal variability to climate-timescale fluctuations. Even though it is incomplete, our current statistical and dynamical understanding of the AMs can be applied in a variety of environmental contexts, including investigation of temperature extremes [*Thompson and Wallace*, 2001], oceanic circulation, the global carbon cycle in the Northern and Southern Hemispheres [e.g. *Russell and Wallace*, 2004; *Butler et al.*, 2007], Antarctic surface climate [e.g. *Thompson and Solomon*, 2002], and many other diverse topics that are outside the scope of this Chapter. Because the AMs represent a characteristic pattern of climate response as well as climate variability, further attention will continue to be warranted as we move forward with attempts to predict the future of evolution of the Earth system.

A key issue that remains unresolved in this discussion is the mechanisms underlying stratosphere-troposphere AM coupling, and the coupling of AMs to the land and ocean surface. We have attempted to clarify those aspects of tropospheric and stratospheric AM variability that can be understood in isolation and those for which surface and stratosphere coupling are more critical. The stratospheric and tropospheric AMs can be regarded dynamically distinct, but they are linked by eddy driven processes that we are only beginning to understand and quantify. Likewise, we are only beginning to understand the role of snow, ocean surface temperatures in the tropics and extratropics, and other surface forcings in generating AM variability. In the effort to understand the various drivers of AM variability, simplified general circulation models with sufficient horizontal and vertical resolution currently provide our main tool to develop theoretical understanding. At each stage, both comprehensive and simplified GCMs have furnished surprising results, especially in relation to AM timescales and AM climate responses. These developments are currently leading to fundamental insights that, we expect, will solidify our understanding of the observed AMs and their climate responses.

Regarding the climate responses themselves, an intensive research effort on the Southern Hemisphere extratropical circulation response to climate change is warranted at this point. A positive Southern Annular Mode (SAM) response to greenhouse gas increases and ozone depletion appears to be a robust signal common to many climate models, and seems to be in agreement with observations in the second half of the 20th century. But there are reasons to expect, based on the long AM timescale bias identified in Section 4, that the models will tend to be correspondingly biased towards overly large amplitude AM responses. Accurately representing the SAM response will become more challenging and critical as the ozone layer recovers, since the climate and ozone forcing signals are expected to produce opposite signed SAM responses [e.g. *Son et al.*, 2010]. This issue will require a systematic attack using the full model hierarchy before it can be fully resolved.

6. APPENDIX

We recall some of the main results of quasi-geostrophic (QG) theory [*Andrews et al.*, 1987, Ch. 3]. The QG equation in log pressure and tangent plane linear Cartesian coordinates is

$$Dq = -X_y + Y_x + f_0\rho_0^{-1}\left(\rho_0 Q/\theta_0 z\right)_z , \quad (11)$$

where the QG potential vorticity (also known as the pseudo potential vorticity) q is defined by

$$q \equiv f_0 + \beta y + \psi_{xx} + \psi_{yy} + \rho_0^{-1}\left(\rho_0 f_0^2 N^{-2}\psi_z\right)_z ,$$

the QG approximation to the advective derivative acting on the QG potential vorticity q is

$$D = \frac{\partial}{\partial t} + u\frac{\partial}{\partial x} + v\frac{\partial}{\partial y},$$

where the static stability $N^2(z)$ is associated with the reference potential temperature $\theta_0(z)$. Some of the remaining notation is explained as follows:

ψ	Geostrophic streamfunction
$(u, v) = (-\psi_y, \psi_x)$	Geostrophic velocity
$\theta_e = f_0\theta_{0z}\psi_z/N^2$	Potential temperature perturbation from reference θ_{0z}
(X, Y)	Momentum dissipation
Q	Diabatic heating on potential temperature.

If we take the zonal mean of (11) and remove the climatological mean of the result we obtain (4) with

$$\overline{S} = -(\overline{X^a})_y + f_0\rho_0^{-1}\left(\rho_0\overline{Q^a}/\theta_{0z}\right)_z . \quad (12)$$

To show why we expect the density weighted volume average of $\overline{S^a}\,\overline{q^a}$ to be negative, we assume

that the momentum forcing is linear drag with timescale τ_m and the diabatic heating is relaxational on timescale τ_r. If the damping timescales are equal, with $\tau_m = \tau_r \equiv \tau$, then $\overline{S^a} = -\tau\overline{q^a}$ and $\overline{S^a} \cdot \overline{q^a} = -\tau(\overline{q^a})^2 \leq 0$ at each point. But if the momentum and thermal damping timescales are different, it is more difficult to find a general result. We find

$$\begin{aligned}\overline{S^a} &= \tau_m^{-1}(\overline{u^a})_y - f_0\tau_r^{-1}\rho_0^{-1}\left(\rho_0\overline{\theta_e^a}/\theta_{0z}\right)_z \\ &= -\tau_m^{-1}(\overline{\psi^a})_{yy} - \tau_r^{-1}\rho_0^{-1}\left[\rho_0 f_0^2 N^{-2}(\overline{\psi^a})_z\right]_z\end{aligned}$$

and

$$\begin{aligned}&\overline{q^a}\cdot\overline{S^a} \\ &= -\left\{\tau_m^{-1}(\overline{\psi^a})_{yy} + \tau_r^{-1}\rho_0^{-1}\left[\rho_0 f_0^2 N^{-2}(\overline{\psi^a})_z\right]_z\right\} \\ &\quad\cdot\left\{(\overline{\psi^a})_{yy} + \rho_0^{-1}\left[\rho_0 f_0^2 N^{-2}(\overline{\psi^a})_z\right]_z\right\} \\ &= -\Big\{\tau_m^{-1}\left[(\overline{\psi^a})_{yy}\right]^2 \\ &\quad +(\tau_m^{-1}+\tau_r^{-1})\rho_0^{-1}(\overline{\psi^a})_{yy}\left[\rho_0 f_0^2 N^{-2}(\overline{\psi^a})_z\right]_z \\ &\quad +\tau_T^{-1}\left[\rho_0^{-1}\left(\rho_0 f_0^2 N^{-2}(\overline{\psi^a})_z\right)_z\right]^2\Big\}\end{aligned}$$

Now the cross term in this expression is proportional to

$$\begin{aligned}&(\overline{\psi^a})_{yy}\left(\rho_0 f_0^2 N^{-2}(\overline{\psi^a})_z\right)_z \\ &= \nabla\cdot\mathbf{G} + \rho_0 f_0^2 N^{-2}[(\overline{\psi^a})_{yz}]^2,\end{aligned}$$

where

$$\begin{aligned}&\mathbf{G} \\ &= \left[-\rho_0 f_0^2 N^{-2}(\overline{\psi^a})_y(\overline{\psi^a})_{zz}, \rho_0 f_0^2 N^{-2}(\overline{\psi^a})_{yy}(\overline{\psi^a})_z\right]\end{aligned}$$

Density weighted averaging corresponds to $\langle f\rangle = \int \rho_0 dV$, and so

$$\begin{aligned}&\left\langle\overline{q^a}\cdot\overline{S^a}\right\rangle \\ &= -\Big\langle\tau_m^{-1}\left[(\overline{\psi^a})_{yy}\right]^2 \\ &\quad +(\tau_m^{-1}+\tau_r^{-1})f_0^2 N^{-2}\left[(\overline{\psi^a})_{yz}\right]^2 \\ &\quad +\tau_r^{-1}\left[\rho_0^{-1}\left(\rho_0 f_0^2 N^{-2}(\overline{\psi^a})_z\right)_z\right]^2\Big\rangle \\ &\quad +(\tau_m^{-1}+\tau_r^{-1})\int\nabla\cdot\mathbf{G}dV.\end{aligned}$$

Thus, $\left\langle\overline{q^a}\cdot\overline{S^a}\right\rangle$ evaluates to a negative quadratic term plus a flux divergence that integrates out to the boundaries. We have not found a simple justification for zeroing out this flux integral, particularly its vertical contribution, and thus we must allow that boundary terms might provide a source of variance of the zonal mean PV independent of eddy feedbacks in (5). But if we choose boundary conditions that zero out this flux, for example considering the set of solutions for which $(\overline{\psi^a}) = 0$ at the boundary, then $\left\langle\overline{q^a}\cdot\overline{S^a}\right\rangle$ will be negative.

The polar cap density-weighted average potential vorticity tendency in (6) is found from (4)

$$\begin{aligned}&<\overline{q_t{}^a}>_p \\ &= \int_{z_B}^{z_T}\int_{y_S}^{y_N} dydz\left[-\rho_0(\overline{u^a})_{yt} + f_0\rho_0(\overline{\theta_e^a})_t/\theta_{0z}\right]\end{aligned}$$

using $\overline{u^a} = 0$ at $y = y_N$, which corresponds to the North Pole. Equation (8) for the eddy fluxes and dissipation is derived similarly, provided we set the meridional component of the EP flux $F_{(y)} = 0$ at the North Pole. To obtain the vertically integrated momentum balance (9) we take $\rho_0\theta_e/\theta_{0z} \to 0$ as $z_T \to \infty$ and use the zonal mean of the standard QG lower-boundary condition

$$D\theta_e = Q \text{ at } z_B = 0;$$

topographic effects are neglected in this expression.

ACKNOWLEDGMENTS. The support of the Natural Sciences and Engineering Research Council of Canada and the Canadian Foundation for Climate and Atmospheric Sciences is gratefully acknowledged. Thanks go to R.A. Plumb and E.P. Gerber for careful reviews; to K. Smith and D.W.J. Thompson for additional helpful comments; and to L. Mudryk for providing Plate 5, V. Limapsuvan for providing Plate 7, and T. Shaw and M. Sigmond for providing the data for Plate 10.

NOTES

1. A mathematically similar argument for the variance of the eddy potential vorticity leads to the classical result that the eddy potential vorticity flux must be down the meridional potential vorticity gradient, i.e. $\left\langle\overline{v'q'}\cdot\overline{q}_y\right\rangle < 0$, in order to maintain eddy variance. The sum of the eddy and zonal mean variance equations is related to conservation of total potential enstrophy.

REFERENCES

Alexander, M. J., S. D. Eckermann, D. Broutman, and J. Ma (2009), Momentum flux estimates for South Georgia Island mountain waves in the stratosphere observed via satellite, *Geophys. Res. Lett.*, *36*, l12816, doi:10.1029/2009GL038587.

Ambaum, M. H. P., B. J. Hoskins, and D. B. Stephenson (2001), Arctic Oscillation or North Atlantic Oscillation, *J. Atmos. Sci.*, *14*, 3495–3507.

Andrews, D. G., J. R. Holton, and C. B. Leovy (1987), *Middle Atmosphere Dynamics*, Academic Press, New York, 489 pp.

Baldwin, M. (2001), Annular modes in global daily surface pressure, *Geophys. Res. Lett.*, *28*, 4114–4118.

Baldwin, M., et al. (2010), Effects of the stratosphere on the troposphere. Chapter 10 in the SPARC CCMVal report on the evaluation of chemistry-climate models, V. Eyring, T. G. Shepherd, D. W. Waugh (Eds.), SPARC Report No. 5, WCRP-132, WMO/TD-No. 1526.

Baldwin, M. P., and T. J. Dunkerton (1999), Propagation of the Arctic Oscillation from the stratosphere to the troposphere, *J. Geophys. Res.*, *104*, 30,937–30,946.

Baldwin, M. P., and T. J. Dunkerton (2001), Stratospheric harbingers of anomalous weather regimes, *Science*, *294*, 581–584.

Baldwin, M. P., and D. W. J. Thompson (2009), A critical comparison of stratosphere-troposphere coupling indices, *Quart. J. Roy. Met. Soc.*, *135*(644), 1661–1672.

Baldwin, M. P., D. B. Stephenson, D. W. J. Thompson, T. J. Dunkerton, A. J. Charlton, and A. O'Neill (2003), Stratospheric memory and skill of extended-range weather forecasts, *Science*, *301*(5633), 636–640.

Baldwin, M. P., D. B. Stephenson, and I. T. Jolliffe (2009), Spatial weighting and iterative projection methods for EOFs, *J. Climate*, *22*, 234–243.

Bell, C. J., L. J. Gray, A. J. Charlton-Perez, M. M. Joshi, and A. A. Scaife (2009), Stratospheric communication of El Niño teleconnections to European winter, *J. Climate*, *22*, 4083–4096.

Boville, B. A. (1984), The influence of the polar night jet on the tropospheric circulation in a GCM, *J. Atmos. Sci.*, *41*, 1132–1142.

Boville, B. A., and X. H. Cheng (1988), Upper boundary effects in a general-circulation model, *J. Atmos. Sci.*, *45*, 2591–2606.

Butler, A. H., D. W. J. Thompson, and K. R. Gurney (2007), Observed relationships between the Southern Annular Mode and atmospheric carbon dioxide, *Global Biogeochem. Cy.*, *21*(4).

Cagnazzo, C., and E. Manzini (2009), Impact of the stratosphere on the winter tropospheric teleconnections between ENSO and the North Atlantic and European region, *J. Climate*, *22*, 1223–1238.

Cai, W. J., and T. Cowan (2007), Trends in Southern Hemisphere circulation in IPCC AR4 models over 1950-99: Ozone depletion versus greenhouse forcing, *J. Climate*, *20*, 681–693.

Cash, B. A., P. J. Kushner, and G. K. Vallis (2002), The structure and composition of the annular modes in an aquaplanet general circulation model., *J. Atmos. Sci.*, *59*, 3399–3414.

Chan, C. J., and R. A. Plumb (2009), The response to stratospheric forcing and its dependence on the state of the troposphere, *J. Atmos. Sci.*, *66*, 2107–2115.

Charlton, A. J., A. O'Neill, W. A. Lahoz, and A. C. Massacand (2004), Sensitivity of tropospheric forecasts to stratospheric initial conditions, *Quart. J. Roy. Met. Soc.*, *130*(600), 1771–1792.

Christiansen, B. (2001), Downward propagation of zonal mean zonal wind anomalies from the stratosphere to the troposphere: Model and reanalysis, *J. Geophys. Res.*, *106*, 27,307–27,322.

Codron, F. (2005), Relation between annular modes and the mean state: Southern Hemisphere Summer, *J. Climate*, *18*(2), 320–330.

Cohen, J., and M. Barlow (2005), The NAO, the AO, and global warming: How closely related?, *J. Climate*, *18*, 4498–4513.

Cohen, J., and D. Entekhabi (1999), Eurasian snow cover variability and Northern Hemisphere climate predictability, *Geophys. Res. Lett.*, *26*, 345–348.

Cohen, J., M. Barlow, P. J. Kushner, and K. Saito (2007), Stratosphere-troposphere coupling and links with Eurasian land surface variability, *J. Climate*, *20*, 5335–5343.

Deser, C. (2000), On the teleconnectivity of the Arctic Oscillation, *Geophys. Res. Lett.*, *27*, 779–782.

Deser, C., G. Magnusdottir, R. Saravanan, and A. Phillips (2004), The effects of North Atlantic SST and sea ice anomalies on the winter circulation in CCM3. Part II: Direct and indirect components of the response, *J. Climate*, *17*, 877–889.

Eichelberger, S. J., and D. L. Hartmann (2007), Zonal jet structure and the leading mode of variability, *J. Climate*, *20*(20), 5149–5163.

Feldstein, S. B. (2000), Is interannual zonal mean flow variability simply climate noise?, *J. Climate*, *13*, 2356–2362.

Fletcher, C. G., S. C. Hardiman, P. J. Kushner, and J. Cohen (2009), The dynamical response to snow cover perturbations in a large ensemble of atmospheric GCM integrations, *J. Climate*, *22*, 1208–1222.

Fogt, R. L., J. Perlwitz, A. J. Monaghan, D. H. Bromwich, J. M. Jones, and G. J. Marshall (2009), Historical SAM variability. Part II: Twentieth-century variability and trends from reconstructions, observations, and the IPCC AR4 models, *J. Climate*, *22*, 5346–5365.

Fyfe, J. C., G. J. Boer, and G. M. Flato (1999), The Arctic and Antarctic oscillations and their projected changes under global warming., *Geophys. Res. Lett.*, *26*, 1601–1604.

Galewsky, J., R. K. Scott, and L. M. Polvani (2004), An initial-value problem for testing numerical models of the global shallow-water equations, *Tellus*, *56*, 429–440.

Garfinkel, C., D. Hartmann, and F. Sassi (2010), Tropospheric precursors of anomalous northern hemisphere stratospheric polar vortices, *Journal of Climate*, pp. 3282–3298.

Garfinkel, C. I., and D. L. Hartmann (2008), Different ENSO teleconnections and their effects on the stratospheric polar vortex, *J. Geophys. Res.*, *113*.

Gerber, E. P., and L. M. Polvani (2009), Stratosphere-troposphere coupling in a relatively simple AGCM: The importance of stratospheric variability, *J. Climate*, *22*, 1920–1933.

Gerber, E. P., and G. K. Vallis (2005), A stochastic model of the spatial structure of the annular patterns of variability and the NAO, *J. Climate*, *18*, 2102–2118.

Gerber, E. P., L. M. Polvani, and D. Ancukiewicz (2008a), Annular mode time scales in the Intergovernmental Panel on Climate Change Fourth Assessment Report models, *Geophys. Res. Lett.*, *35*, l22707, doi: 10.1029/2008GL035712.

Gerber, E. P., S. Voronin, and L. M. Polvani (2008b), Testing the annular mode autocorrelation time scale in simple atmospheric general circulation models, *Mon. Weather Rev.*, *136*, 1523–1536.

Gillett, N. P., and D. Thompson (2003), Simulation of recent Southern Hemisphere climate change, *Science*, *302*, 273–275.

Gillett, N. P., M. R. Allen, and K. D. Williams (2002), The role of stratospheric resolution in simulating the Arctic Oscillation response to greenhouse gases, *Geophys. Res. Lett.*, *29*, 138-1-138-4, doi: 10.1029/2001GL014444.

Gong, D., and S. Wang (1999), Definition of Antarctic Oscillation index, *Geophys. Res. Lett.*, *26*, 459–462.

Gong, G., D. Entekhabi, and J. Cohen (2002), A large-ensemble model study of the wintertime AO-NAO and the role of interannual snow perturbations, *J. Climate*, *15*, 3488–3499.

Gritsun, A., and G. Branstator (2007), Climate response using a three-dimensional operator based on the fluctuation-dissipation theorem, *J. Atmos. Sci.*, *64*, 2558–2575.

Hardiman, S. C., and P. H. Haynes (2008), Dynamical sensitivity of the stratospheric circulation and downward influence of upper level perturbations, *J. Geophys.Res.*, *113*.

Hardiman, S. C., P. J. Kushner, and J. Cohen (2008), Investigating the ability of general circulation models to capture the effects of Eurasian snow cover on winter climate, *J. Geophys. Res.*, *113*.

Hartmann, D., J. Wallace, V. Limpasuvan, D. Thompson, and J. Holton (2000), Can ozone depletion and greenhouse warming interact to produce rapid climate change?, *Proc. Nat. Acad. Sci.*, *97*, 1412–1417.

Haynes, P. H., M. E. McIntyre, T. G. Shepherd, C. J. Marks, and K. P. Shine (1991), On the "downward control" of extratropical diabatic circulations by eddy-induced mean zonal forces., *J. Atmos. Sci.*, *48*, 651–680.

Held, I. M. (2005), The gap between simulation and understanding in climate modeling, *Bull. Amer. Met. Soc.*, *86*, 1609–1614.

Held, I. M., and M. J. Suarez (1994), A proposal for the intercomparison of the dynamical cores of atmospheric general circulation models, *Bull. American Met. Soc.*, *75*, 1825–1830.

Holton, J. R., and C. Mass (1976), Stratospheric vacillation cycles, *J. Atmos. Sci.*, *33*, 2218–2225.

Hoskins, B. J., M. E. McIntyre, and A. W. Robertson (1985), On the use and significance of isentropic potential vorticity maps, *Quart. J. Roy. Met. Soc.*, *111*(470), 877–946.

Hu, Y., and K. K. Tung (2002), Interannual and decadal variations of planetary-wave activity, stratospheric cooling, and the Northern-Hemisphere Annular Mode., *J. Climate*, *15*, 1659–1673.

Ineson, S., and A. A. Scaife (2009), The role of the stratosphere in the European climate response to El Niño, *Nature Geo.*, *2*, 32–36.

Kalnay, E., et al. (1996), The NCEP/NCAR 40-year reanalysis project, *Bull. Amer. Met. Soc.*, *77*(3), 437–471.

Karpechko, A. Y., N. P. Gillett, G. J. Marshall, and J. A. Screen (2009), Climate impacts of the Southern Annular Mode simulated by the CMIP3 models, *J. Climate*, *22*, 3751–3768.

Kidston, J., and E. Gerber (2010), Intermodel variability of the poleward shift of the austral jet stream in the CMIP3 integrations linked to biases in 20th century climatology, *Geophys. Res. Lett.*, *37*, doi:10.1029/2010GL042,873.

Kim, H., and S. Lee (2001), Hadley cell dynamics in a primitive equation model. part ii: Nonaxisymmetric flow, *J. Atmos. Sci.*, *58*, 2859–2871.

Kodera, K., K. Yamazaki, M. Chiba, and K. Shibata (1990), Downward propagation of upper stratospheric mean zonal wind perturbation to the troposphere, *Geophys. Res. Lett.*, *17*, 1263–1266.

Kushner, P., and L. Polvani (2004), Stratosphere-troposphere coupling in a relatively simple AGCM: The role of eddies, *J. Clim.*, *17*, 629–639.

Kushner, P., I. M. Held, and T. L. Delworth (2001), Southern-Hemisphere atmospheric circulation response to global warming, *J. Climate*, *14*, 22,380–2249.

Kushner, P. J., and G. Lee (2007), Resolving the regional signature of the annular modes, *J. Climate*, *20*, 2840–2852.

Lee, S., and S. B. Feldstein (1996), Mechanism of zonal index evolution in a two-layer model, *J. Atmos. Sci.*, *53*, 2232–2246.

Lee, S., and H. Kim (2003), The dynamical relationship between subtropical and eddy-driven jets, *J. Atmos. Sci.*, *60*, 1490–1503.

Leith, C. E. (1975), Climate response and fluctuation dissipation, *J. Atmos. Sci.*, *32*, 2022–2026.

Limpasuvan, V., and D. L. Hartmann (1999), Eddies and the annular modes of climate variability, *Geophys. Res. Lett.*, *26*(20), 3133–3136.

Limpasuvan, V., and D. L. Hartmann (2000), Wave-maintained annular modes of climate variability, *J. Climate*, *13*, 4414–4429.

Limpasuvan, V., D. W. J. Thompson, and D. L. Hartmann (2004), The life cycle of the northern hemisphere sudden stratospheric warmings, *J. Climate*, *17*, 2584–2596.

Limpasuvan, V., D. L. Hartmann, D. W. J. Thompson, K. Jeev, and Y. L. Yung (2005), Stratosphere-troposphere evolution during polar vortex intensification, *J. Geophys. Res.*, *110*.

Lorenz, D. J., and D. L. Hartmann (2001), Eddy-zonal flow feedback in the Southern Hemisphere, *J. Atmos. Sci.*, *58*, 3312–3327.

Lorenz, D. J., and D. L. Hartmann (2003), Eddy-zonal flow feedback in the Northern Hemisphere winter, *J. Climate*, *16*(8), 1212–1227.

McLandress, C., and J. F. Scinocca (2005), The GCM response to current parameterizations of nonorographic gravity wave drag, *J. Atmos. Sci.*, *62*, 2394–2413, part 2.

Miller, R. L., G. A. Schmidt, and D. T. Shindell (2006), Forced annular variations in the 20th century Intergovernmental Panel on Climate Change Fourth Assessment Report models, *J. Geophys. Res.*, *111*.

Monahan, A. H., and J. C. Fyfe (2006), On the nature of zonal jet EOFs, *J. Climate*, *19*, 6409–6424.

Newman, P. A., E. R. Nash, and J. Rosenfield (2001), What controls the temperature of the Arctic stratosphere during the spring?, *J. Geophys. Res.*, *106*, 19,999–20,010.

Overland, J. E., and M. Wang (2005), The Arctic climate paradox: The recent decrease of the Arctic Oscillation, *Geophys. Res. Lett.*, *32*.

Palmer, T. N. (1999), A nonlinear dynamical perspective on climate prediction, *J. Climate*, *12*, 575–591.

Panetta, R. (1993), Zonal jets in wide baroclinically unstable regions: Persistence and scale selection, *J. Atmos. Sci.*, *50*, 20732106.

Perlwitz, J., and H.-F. Graf (1995), The statistical connection between tropospheric and stratospheric circulation of the Northern Hemisphere in winter, *J. Climate*, *8*, 2281–2295.

Perlwitz, J., S. Pawson, R. L. Fogt, J. E. Nielsen, and W. D. Neff (2008), Impact of stratospheric ozone hole recovery on Antarctic climate, *Geophys. Res. Lett.*, *35*, l08714, doi:10.1029/2008GL033317.

Plumb, R., and K. Semeniuk (2003), Downward migration of extratropical zonal wind anomalies, *J. Geophys. Res.*, *108*, 4223.

Polvani, L. M., and P. Kushner (2002), Tropospheric response to stratospheric perturbations in a relatively simple general circulation model, *Geophys. Res. Lett.*, *29*, **18**–1–**18**–4.

Polvani, L. M., and D. W. Waugh (2004), Upward wave activity flux as a precursor to extreme stratospheric events and subsequent anomalous surface weather regimes, *J. Climate*, *17*, 3548–3554.

Ring, M. J., and R. A. Plumb (2007), Forced annular mode patterns in a simple atmospheric general circulation model, *J. Atmos. Sci.*, *64*, 3611–3626.

Ring, M. J., and R. A. Plumb (2008), The response of a simplified GCM to axisymmetric forcings: Applicability of the fluctuation-dissipation theorem, *J. Atmos. Sci.*, *65*, 3880–3898.

Robinson, W. A. (1991), The dynamics of low-frequency variability in a simple-model of the global atmosphere, *J. Atmos. Sci.*, *48*, 429–441.

Robinson, W. A. (2000), A baroclinic mechanism for the eddy feedback on the zonal index, *J. Atmos. Sci.*, *57*, 415–422.

Russell, J. L., and J. M. Wallace (2004), Annual carbon dioxide drawdown and the Northern Annular Mode, *Global Biogeochem. Cy.*, *18*, GB1012, doi:10.1029/2003GB002044.

Scaife, A. A., and J. R. Knight (2008), Ensemble simulations of the cold European winter of 2005-2006, *Quart. J. Roy. Met. Soc.*, *134*, 1647–1659.

Scinocca, J. F., and P. Haynes (1997), Dynamical forcing of stratospheric planetary waves by tropospheric baroclinic eddies., *J. Atmos. Sci.*, *55*, 2361–2392.

Scott, R. K., and L. M. Polvani (2006), Internal variability of the winter stratosphere. Part I: Time-independent forcing., *J. Atmos. Sci.*, *63*, 2758–2776.

Sexton, D. M. H. (2001), The effect of stratospheric ozone depletion on the phase of the Antarctic Oscillation., *Geophys. Res. Lett.*, *28*, 3697–3700.

Shaw, T. A., M. Sigmond, T. G. Shepherd, and J. F. Scinocca (2009), Sensitivity of simulated climate to conservation of momentum in gravity wave drag parameterization, *J. Climate*, *22*, 2726–2742.

Shindell, D. T., R. L. Miller, G. Schmidt, , and L. Pandolfo (1999), Simulation of recent Northern winter climate trends by greenhouse-gas forcing, *Nature*, *399*, 452–455.

Shindell, D. T., G. A. Schmidt, R. L. Miller, and D. Rind (2001), Northern Hemisphere winter climate response to greenhouse gas, ozone, solar, and volcanic forcing, *J. Geophys. Res.*, *106*, 7193–7210.

Sigmond, M., J. F. Scinocca, and P. J. Kushner (2008), Impact of the stratosphere on tropospheric climate change, *Geophys. Res. Lett.*, *35*, L12706, doi:10.1029/2008GL033573.

Son, S. W., et al. (2008), The impact of stratospheric ozone recovery on the Southern Hemisphere westerly jet, *Science*, *320*, 1486–1489.

Son, S.-W., et al. (2010), The impact of stratospheric ozone on southern hemisphere circulation change: A multimodel assessment, *J. Geophys. Res.*, p. In press.

Song, Y., and W. A. Robinson (2004), Dynamical mechanisms for stratospheric influences on the troposphere, *J. Atmos. Sci.*, *61*, 1711–1725.

Taguchi, M., and S. Yoden (2002), Internal interannual variations of the troposphere- stratosphere coupled system in a simple global circulation model. Part I: Parameter sweep experiment, *J. Atmos. Sci.*, *59*, 3021–3036.

Thompson, D. W. J., and S. Solomon (2002), Interpretation of recent Southern Hemisphere climate change, *Science*, *296*, 895–899.

Thompson, D. W. J., and J. M. Wallace (1998), The Arctic Oscillation signature in the wintertime geopotential height and temperature fields, *Geophys. Res. Lett.*, *25*, 1297–1300.

Thompson, D. W. J., and J. M. Wallace (2000), Annular modes in the extratropical circulation. Part I: Month-to-month variability, *J. Climate*, *13*, 1000–1016.

Thompson, D. W. J., and J. M. Wallace (2001), Regional climate impacts of the Northern Hemisphere annular mode, *Science*, *293*, 85–89.

Thompson, D. W. J., J. M. Wallace, and G. C. Hegerl (2000), Annular modes in the extratropical circulation. Part II: Trends., *J. Climate*, *13*, 1018–1036.

Vallis, G. K. (2006), *Atmospheric and Oceanic Fluid Dynamics*, p. 745, Cambridge University Press, Cambridge, UK.

Vallis, G. K., E. P. Gerber, P. J. Kushner, and B. A. Cash (2004), A mechanism and simple dynamical model of the North Atlantic Oscillation and annular modes., *J. Atmos. Sci.*, *61*, 264–280.

Walker, C. C., and T. Schneider (2009), Eddy influences on hadley circulations: Simulations with an idealized gcm, *J. Atmos. Sci.*

Wallace, J. M. (2000), North Atlantic Oscillation/annular mode: Two paradigms - one phenomenon, *Quart. J. Roy. Meteorol. Soc.*, *126*(564), 791–805.

Wallace, J. M., and D. W. J. Thompson (2002), The Pacific center of action of the Northern Hemisphere annular mode: Real or artifact?, *J. Climate*, *15*(14), 1987–1991.

Wolter, K., and M. Timlin (1993), Monitoring ENSO in COADS with a seasonally adjusted principal component index., in *Proc. of the 17th Climate Diagnostics Workshop*, pp. 52–57, Norman, OK, NOAA/NMC/CAC, NSSL, Oklahoma Clim. Survey, CIMMS and the School of Meteor., Univ. of Oklahoma.

Yoden, S. (1987), Dynamical aspects of stratospheric vacillations in a highly truncated model, *J. Atmos. Sci.*, *44*, 3683–3695.

Yu, J.-Y., and D. L. Hartmann (1993), Zonal flow vacillation and eddy forcing in a simple GCM of the atmosphere., *J. Atmos. Sci.*, *50*, 3244–3259.

Paul J. Kushner, Department of Physics, University of Toronto, 60 St. George St., Toronto, ON, M5S 1A7, Canada

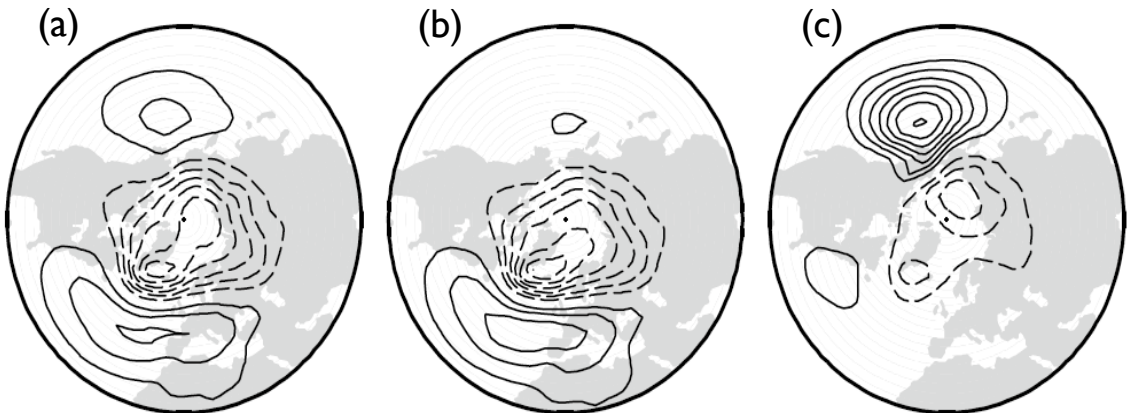

Figure 1. Regression of SLP on principal component time series from EOF analysis of SLP in three domains: (a) the domain poleward of 20^0N for the Northern Hemisphere. (b), as in (a), for the North Atlantic sector. (c), as in (a), for the North Pacific sector. Adapted from *Deser* [2000].

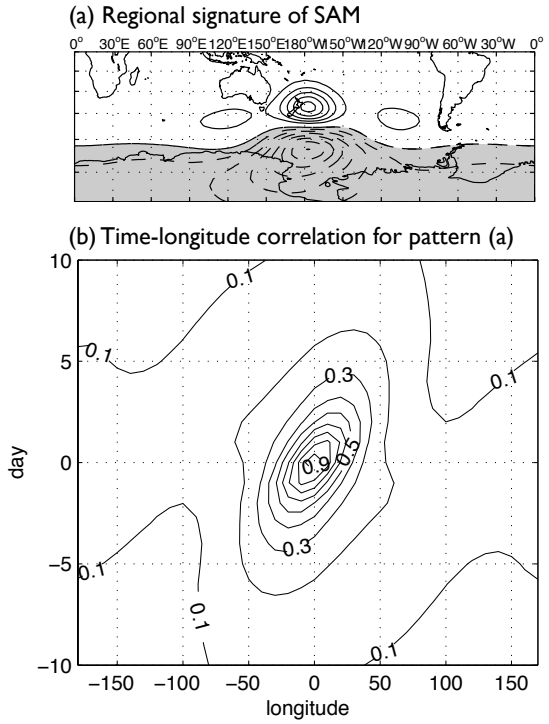

Figure 2. (a) Composite regression pattern for local dipole index on daily surface pressure. The local dipole index represents the principal component time series for the second EOF of surface pressure at a single longitude. The regression with two dimensional surface pressure is calculated for each longitude, shifted to a common longitude for plotting purposes, and averaged. Thus, the geographic boundaries are provided for a sense of scale only. Contour interval: 1 hPa. (b) Longitude-time lag correlation plot of Southern Hemisphere dipole indexes associated with the pattern in (a). The dipoles progate eastward as coherent packets in both hemispheres with a characteristic speed of about 8 degrees longitude per day. Contour interval 0.1. From *Kushner and Lee* [2007].

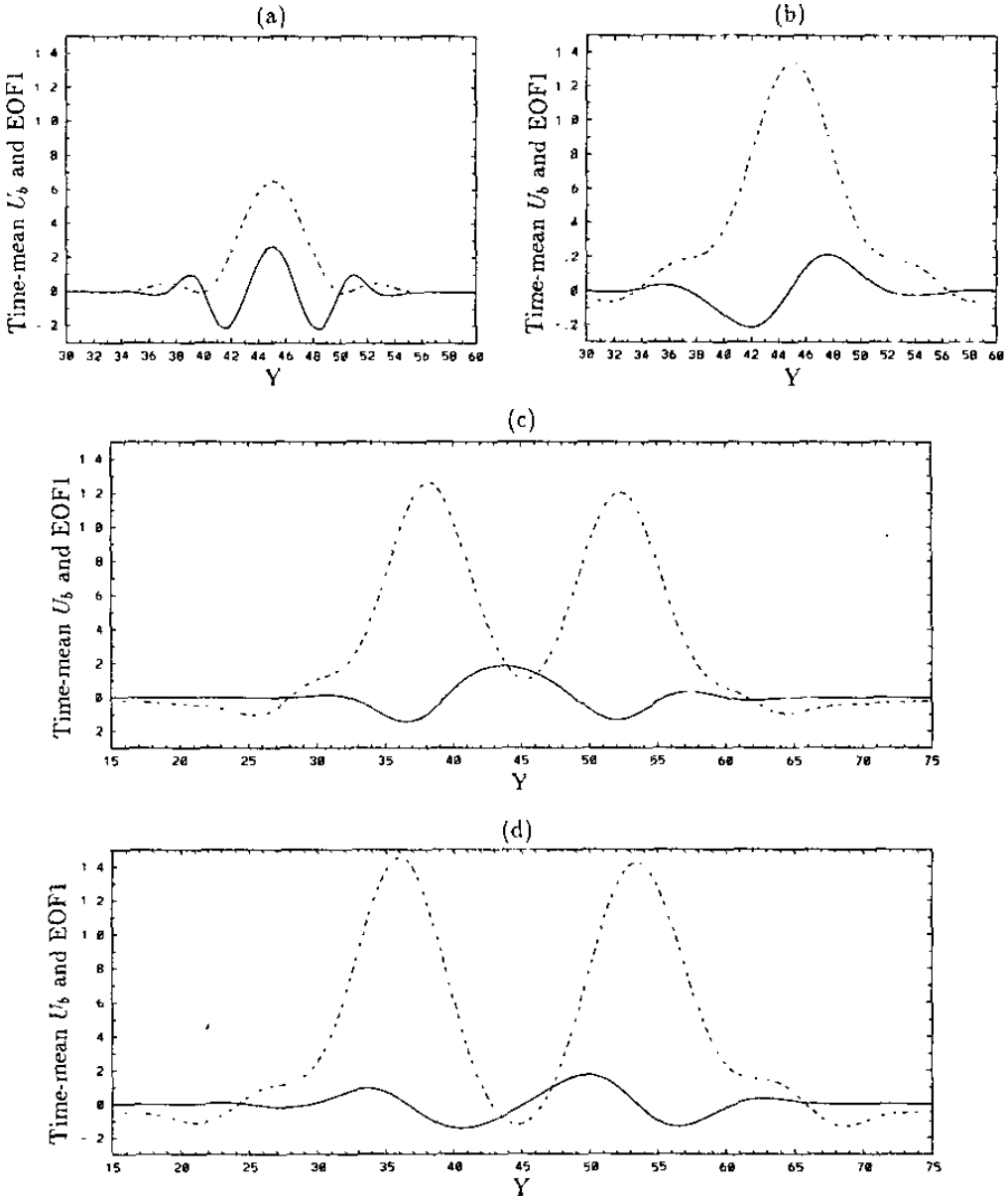

Figure 3. Two-layer quasigeostrophic model simulation of dependence of leading EOF of zonal wind variability (solid) on width of baroclinic zone as represented by the zonal mean zonal wind (dotted) [*Lee and Feldstein*, 1996]. The baroclinic zone is progressively widened proceeding from panel (a) to (d); between panels (b) and (c) the zonal mean wind transitions from a single-jet to a two-jet structure.

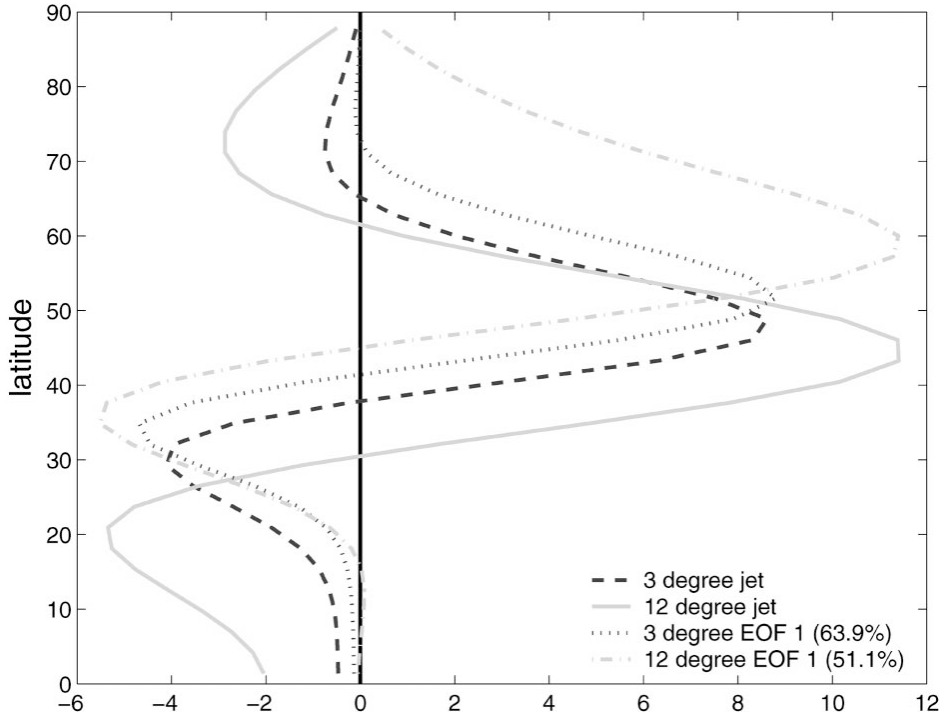

4

Figure 4. Latitude dependence of the zonal mean zonal wind ("jet") and the leading mode of variability of the zonal mean zonal wind ("EOF 1") in a stochastically stirred barotropic model [*Vallis et al.*, 2004]. Results from simulations in which the stirring region is 3 degrees latitude wide and 12 degrees latitude wide are shown. The narrow 3-degree jet has a "pulsing" EOF; the wider 12-degree jet has "wobbling" EOF that corresponds to the AM.

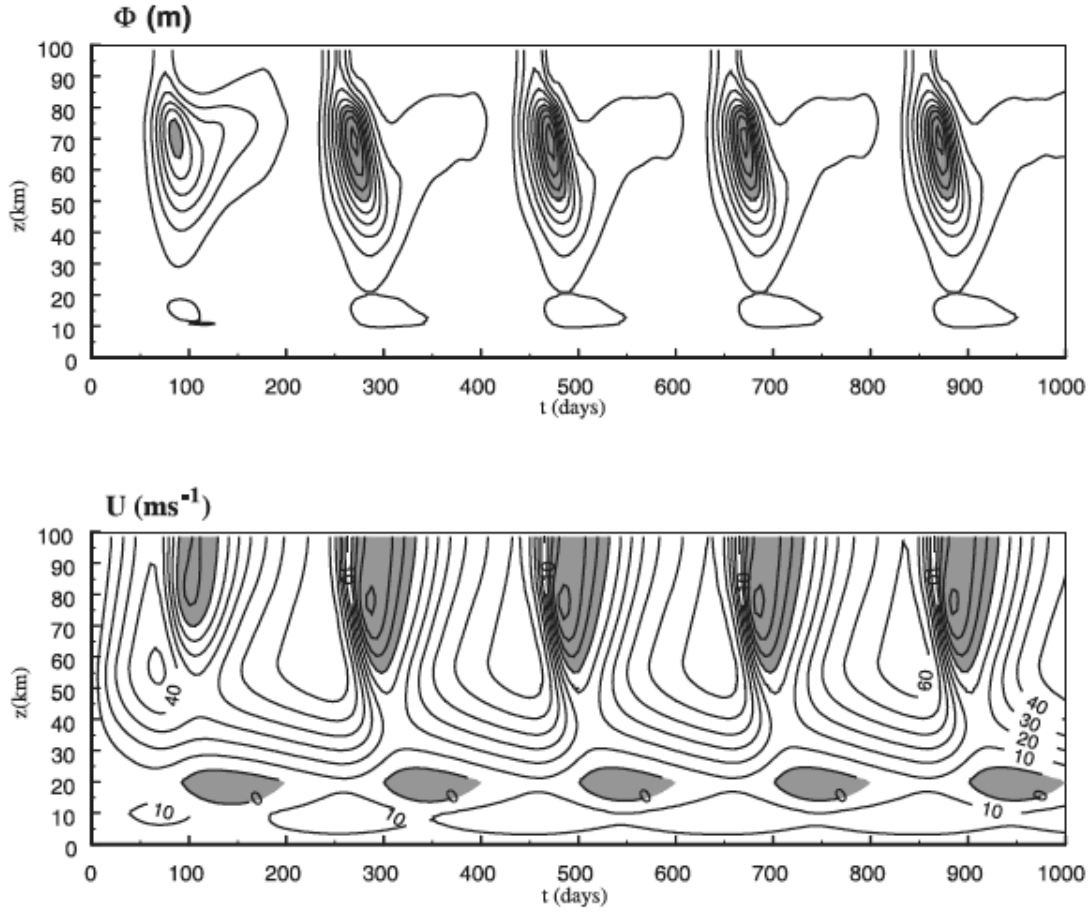

Figure 5. Response in geopotential and zonal wind of a simple Holton-Mass β-channel stratospheric model to periodic forcing from the troposphere. The model represents extratropical eddy mean flow interactions from upward propagating Rossby waves generated by a prescribed zonally asymmetric lower boundary. The prescribed forcing has a period of 200 d. From *Plumb and Semeniuk* [2003].

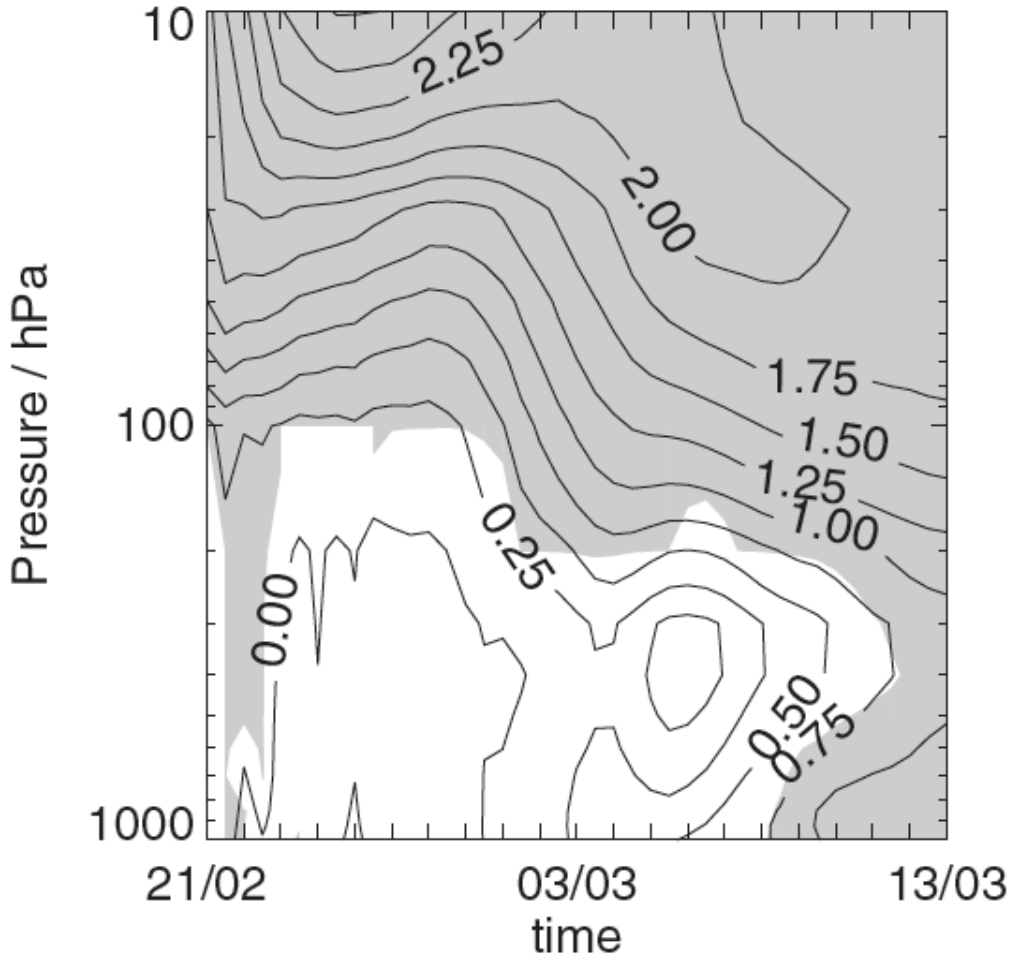

Figure 6. Ensemble mean NAM response to switch on strengthening of stratospheric polar vortex, introduced by means of changing stratospheric initial state. The initial tropospheric response in the first two days arises from an adjustment to a new balanced state in the stratosphere. The positive NAM response, which occurs after a delay of about two weeks, is the result of changes to the stratospheric state. From *Charlton et al.* [2004].

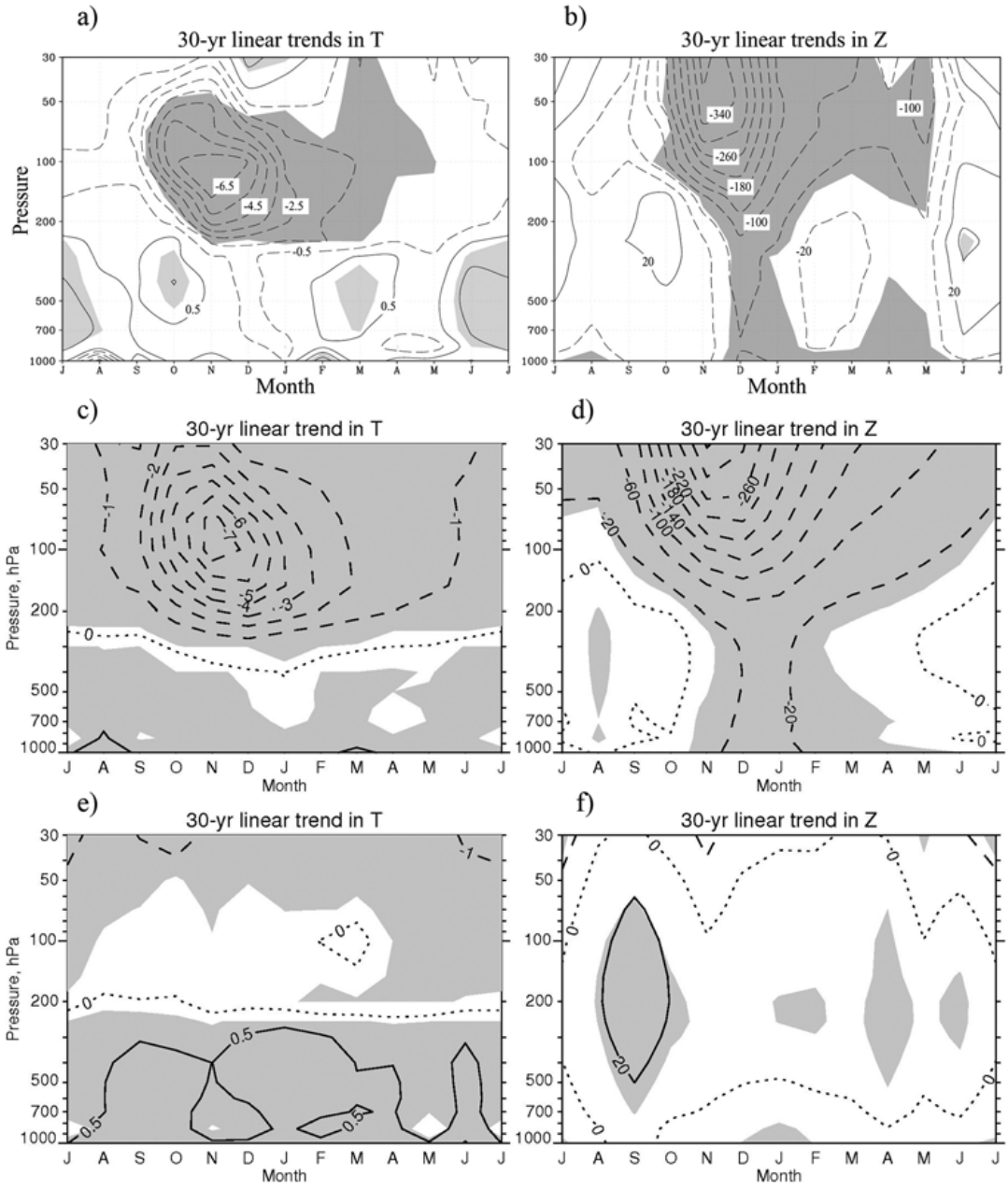

Figure 7. Antarctic trends for 1968-1999 in (left) temperature (K per 30 years) and (right) geopotential height (m per 30 years) as a function of calendar month and pressure for observations (a)-(b), ensemble mean of CMIP3/IPCC AR4 models that include the effects of ozone depletion (c)-(d), and ensemble mean of the models that do not include the effects of ozone depletion (e)-(f), from *Karpechko et al.* [2009]. Averages use points corresponding to the stations from *Thompson and Solomon* [2002]. This and other studies (e.g. *Cai and Cowan* [2007]) confirm that ozone depletion is responsible for at least half of the 1968-1999 trend in the SAM in the troposphere.

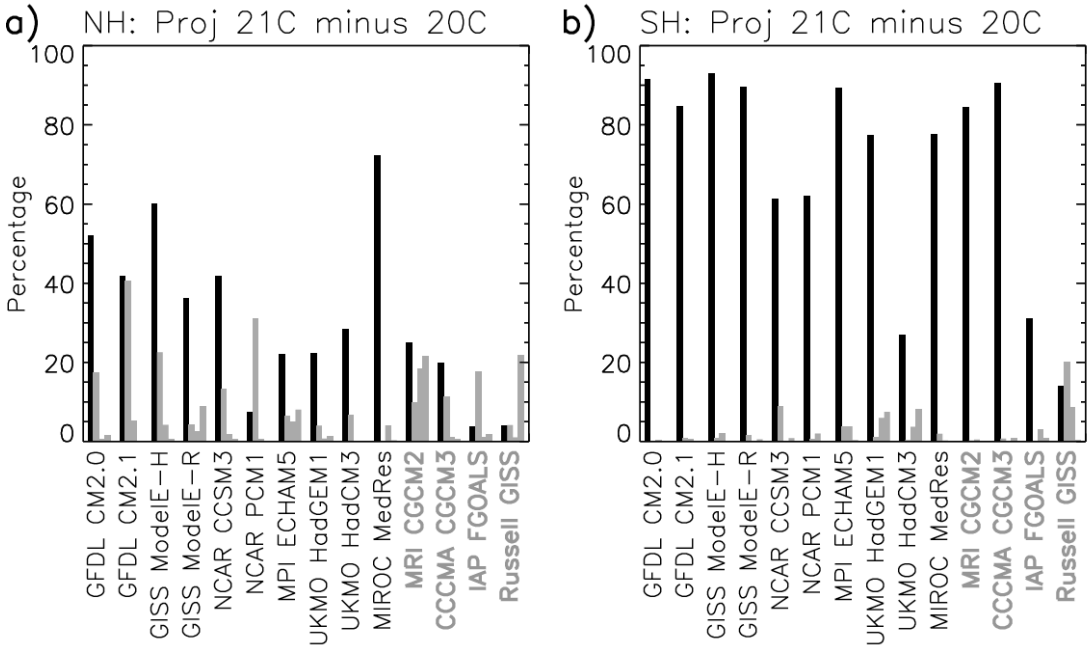

Figure 8. From *Miller et al.* [2006]: (a) Percentage of variance represented by projection of SLP trends in the 20th century onto four leading modes of extratropical variability in the CMIP3/IPCCAR4 models, for the Northern Hemisphere. (b) As in (a), for the Southern Hemisphere.

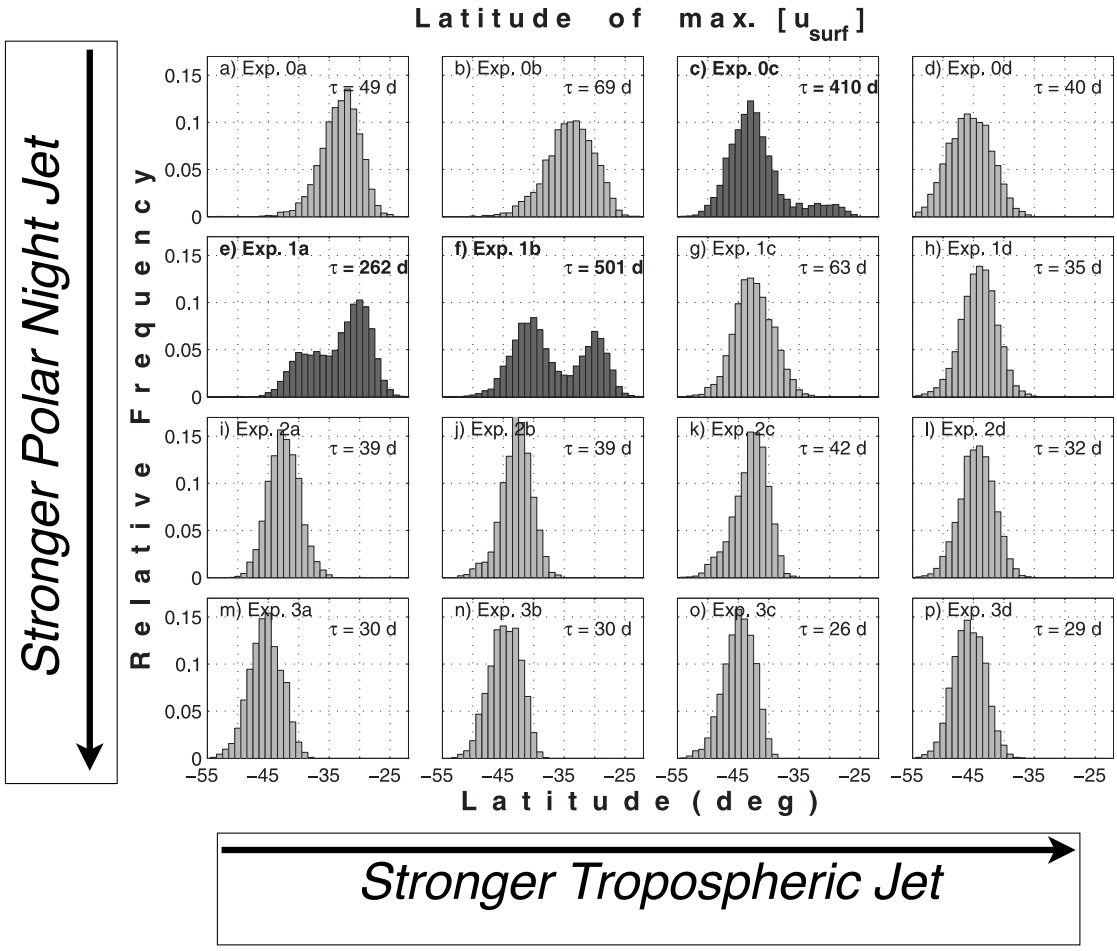

Figure 9. Frequency distribution of meridional location of the tropospheric jet maximum in a simplified GCM for increasingly cold polar stratosphere (increasingly strong polar vortex), going left to right in each row, and for increasingly strong tropospheric meridional temperature gradient, going from top to bottom in each column. Going from weak to strong tropospheric temperature gradient and stratospheric polar vortex, the jet variability passes from a subtropical regime to an extratropical regime, through a mixed bimodal regime. In the mixed regime, the jet can be found in either an extratropical or a subtropical location, and can persist in one of these locations for a long period of time; the darker bars indicate high-persistence regimes with the marked timescales τ. In addition, in the mixed regime, the jet is relatively sensitive to stratospheric cooling. In the extratropically trapped regime, the sensitivity to the stratosphere is attenuated or vanishes. Adapted from *Chan and Plumb* [2009].

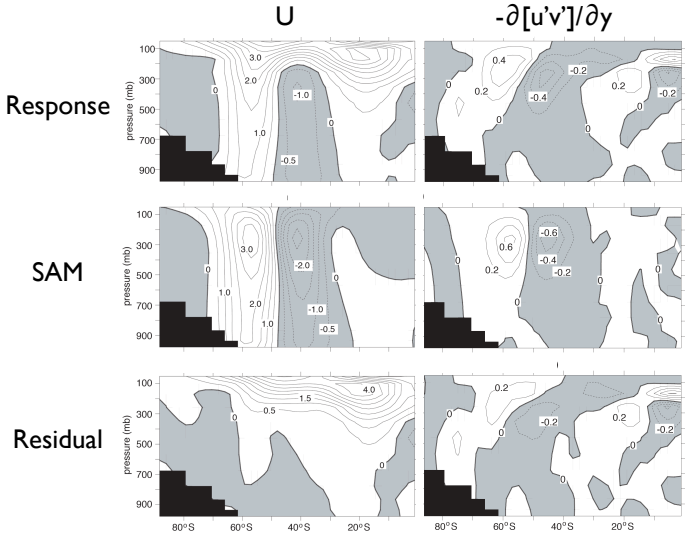

Figure 10. Analysis of zonal wind response (left column) and eddy momentum flux convergence response (right column) to greenhouse warming in the GFDL R30 model, from *Kushner et al.* [2001]. The top row shows the response, the middle row shows the part of the response that is coherent with SAM variability based on the model's lower tropospheric winds, and the bottom row shows the residual (top row minus middle row). The residual is confined to the upper troposphere and lower stratosphere, which *Kushner et al.* [2001] suggest is the location of the strongest forcing of the meridional temperature gradients in the response to climate change; they thus interpret this as the *direct* response to climate change. The SAM related response, on the other hand, involves the eddy-driven SAM variability that is interpreted to be stimulated by the direct forcing; they thus call this the *indirect* response to climate change.

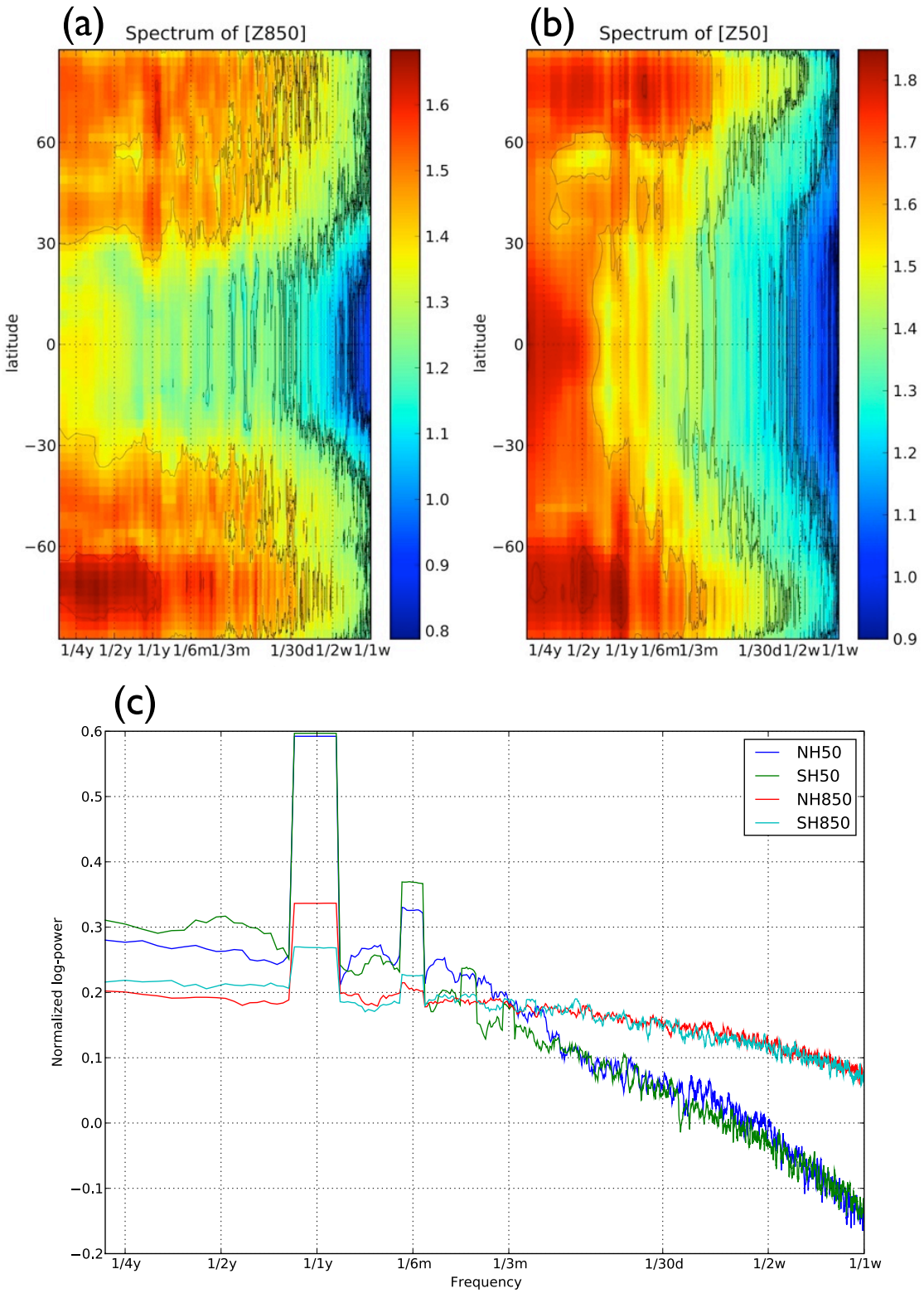

Plate 1. (a) Log of the power spectrum of the zonal mean geopotential anomaly $\tilde{Z}$ from (3) at $p = 850\,\mathrm{hPa}$. Units are arbitrary. The data used is NCEP/NCAR reanalysis [*Kalnay et al.*, 1996] daily averaged geopotential from 1979 to 2008. A simple five point running mean across frequencies has been applied to create smoother plots. (b) As in (a), for $p = 50\,\mathrm{hPa}$. (c) Meridional mean of the log-spectra in (a) and (b) poleward of 22 degrees latitude, scaled to have equal area under each curve.

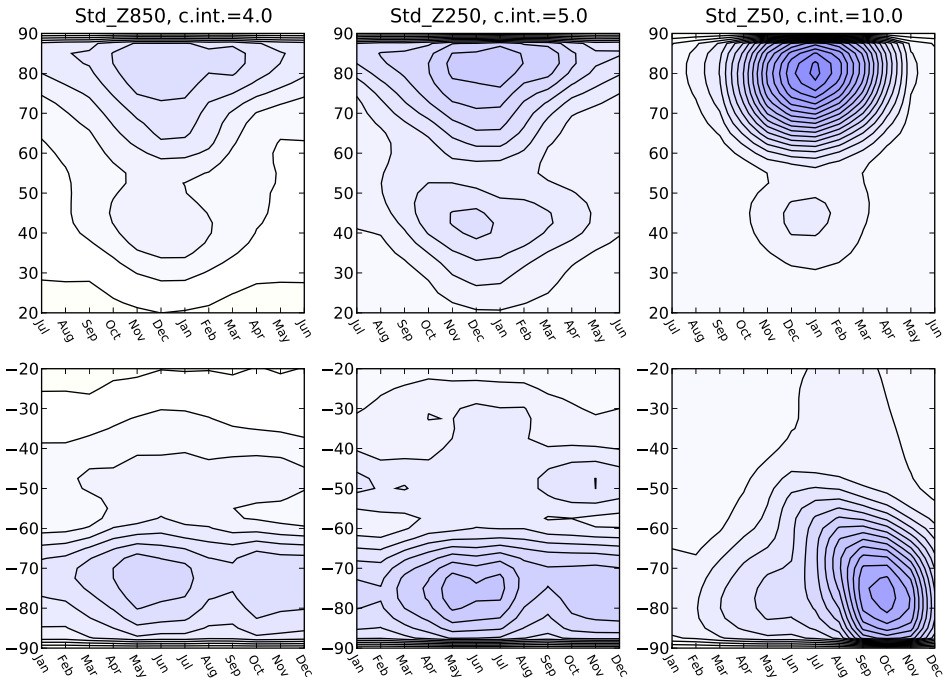

Plate 2. Seasonal cycle of the standard deviation of the seasonal time series of the zonal mean geopotential anomaly $\tilde{Z}_{\rm mon}$ at 850 hPa (left column, contour interval 4 m), 250 hPa (middle column, contour interval 5 m) and 50 hPa (right hand column, contour interval 10 m), for the Northern Hemisphere and Southern Hemisphere extratropics. Calendar months are arranged so that winter solstice is at the center of each panel.

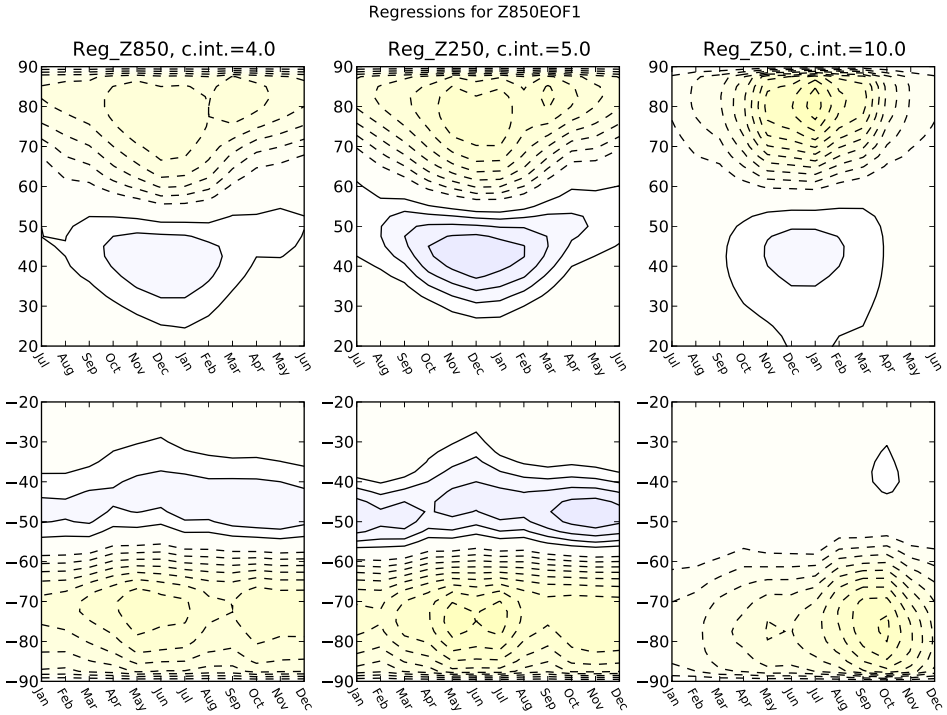

Plate 3. Regressions on the 850 hPa NAM (top row) and the 850 hPa SAM (bottom row) of $\tilde{\mathbf{X}} = \tilde{Z}_{\mathrm{mon}}$ at 850 hPa (left column), $\tilde{\mathbf{X}} = \tilde{Z}_{\mathrm{mon}}$ at 250 hPa (middle column), and $\tilde{\mathbf{X}} = \tilde{Z}_{\mathrm{mon}}$ at 50 hPa (right column). Contour intervals and format as in Plate 2

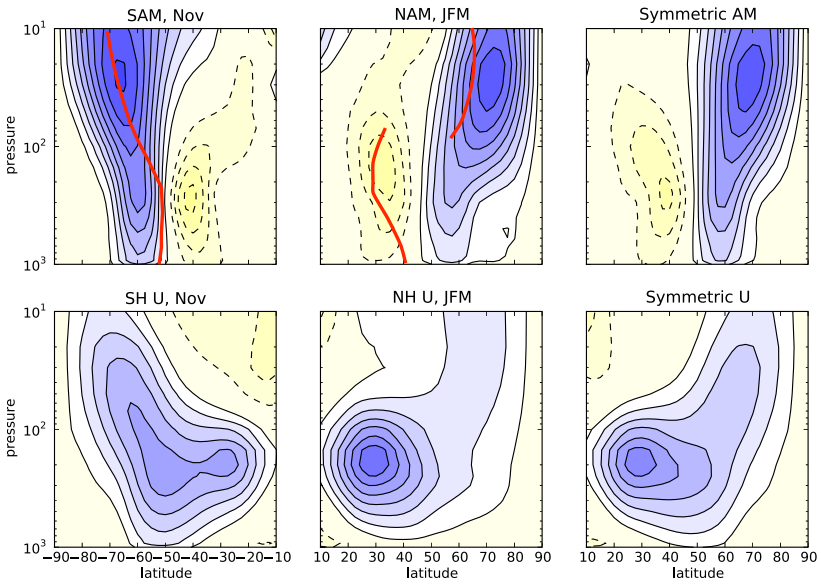

Plate 4. Top row: AM zonal wind regression patterns for Southern Hemisphere November 850 hPa SAM (left), Northern Hemisphere JFM 850 hPa NAM (middle) and the hemispherically symmetric component of these two patterns (right). Bottom row: climatological mean zonal wind for November (left), JFM (middle), and the hemispherically symmetric component of these two patterns (right). The red curves in the top left panels indicate the approximate location of the jet axis in each hemisphere. Contour interval in top row is 0.5 m/s and in bottom row is 5 m/s.

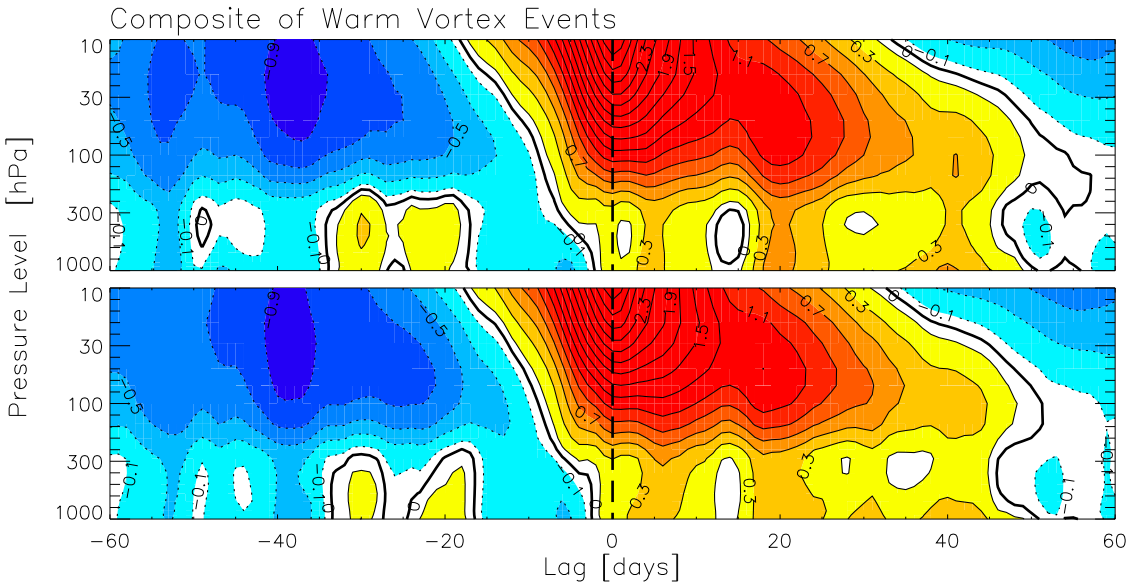

Plate 5. Composites of 50 warm vortex events based on NCEP reanalysis data from 1958-2007. For each winter season (NDJFM) the strongest geopotential height anomaly at 10hPa was used. Contour intervals are spaced by 0.2. Index values between -0.1 and 0.1 are unshaded. The zero level is shown by the heavy black contour. The top panel shows a composite of nondimensional NAM index (based on geopotential height anomalies, and using the zonal-mean EOF method described in *Baldwin and Thompson* [2009]). The bottom panel shows a composite for the time series of polar-cap averaged geopotential height (60^0N-90^0N), normalized by its standard deviation at each level. Figure courtesy of L. Mudryk.

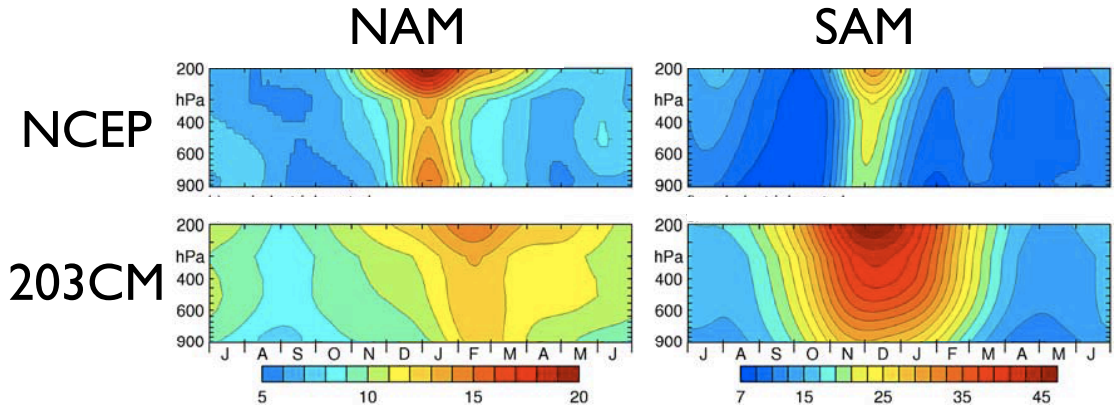

Plate 6. The seasonal cycle of NAM and SAM timescales, computed with the methods of *Baldwin et al.* [2003], for NCEP reanalysis (top row) and for 20th century integrations of coupled climate models in the Fourth Assessment Report of the Intergovernmental Panel on Climate Change (bottom row). Adapted from *Gerber et al.* [2008a].

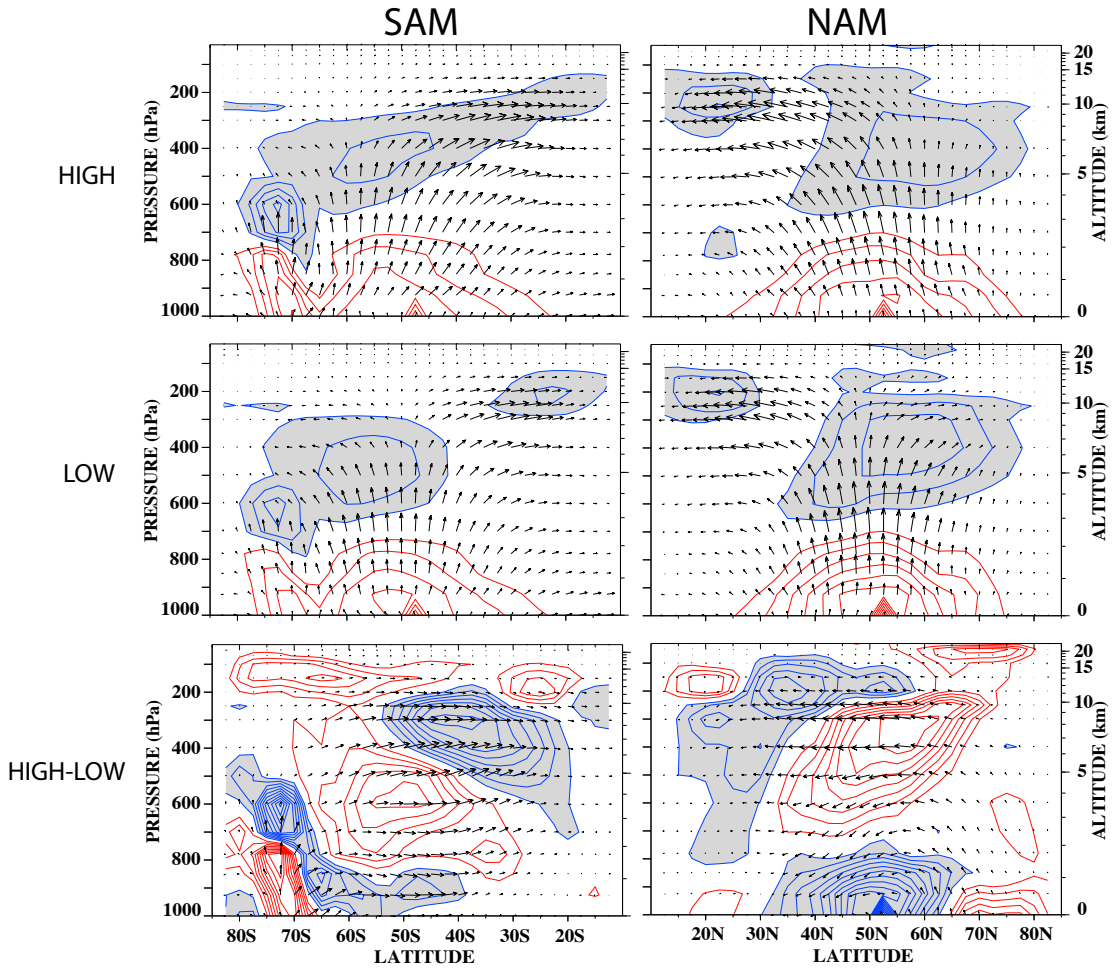

Plate 7. Composite E-P flux cross sections for high and low AM conditions in each hemisphere, and their difference. Contouring indicates regions of EP flux divergence/convergence, with shaded regions indicating EP flux convergence. Contour interval for the top two rows is 1.5 $\mathrm{m\,s^{-1}\,day^{-1}}$, and for the bottom row is 0.25 $\mathrm{m\,s^{-1}\,day^{-1}}$. Negative values (associated with westward acceleration) are shaded and the zero contour is omitted. Eliassen-Palm flux vectors divided by the background density) are shown; the longest vector is about $1.4{\times}10^8\,\mathrm{m^3 s^{-2}}$. Figure courtesy of V. Limpasuvan, adapted from *Limpasuvan and Hartmann* [2000].

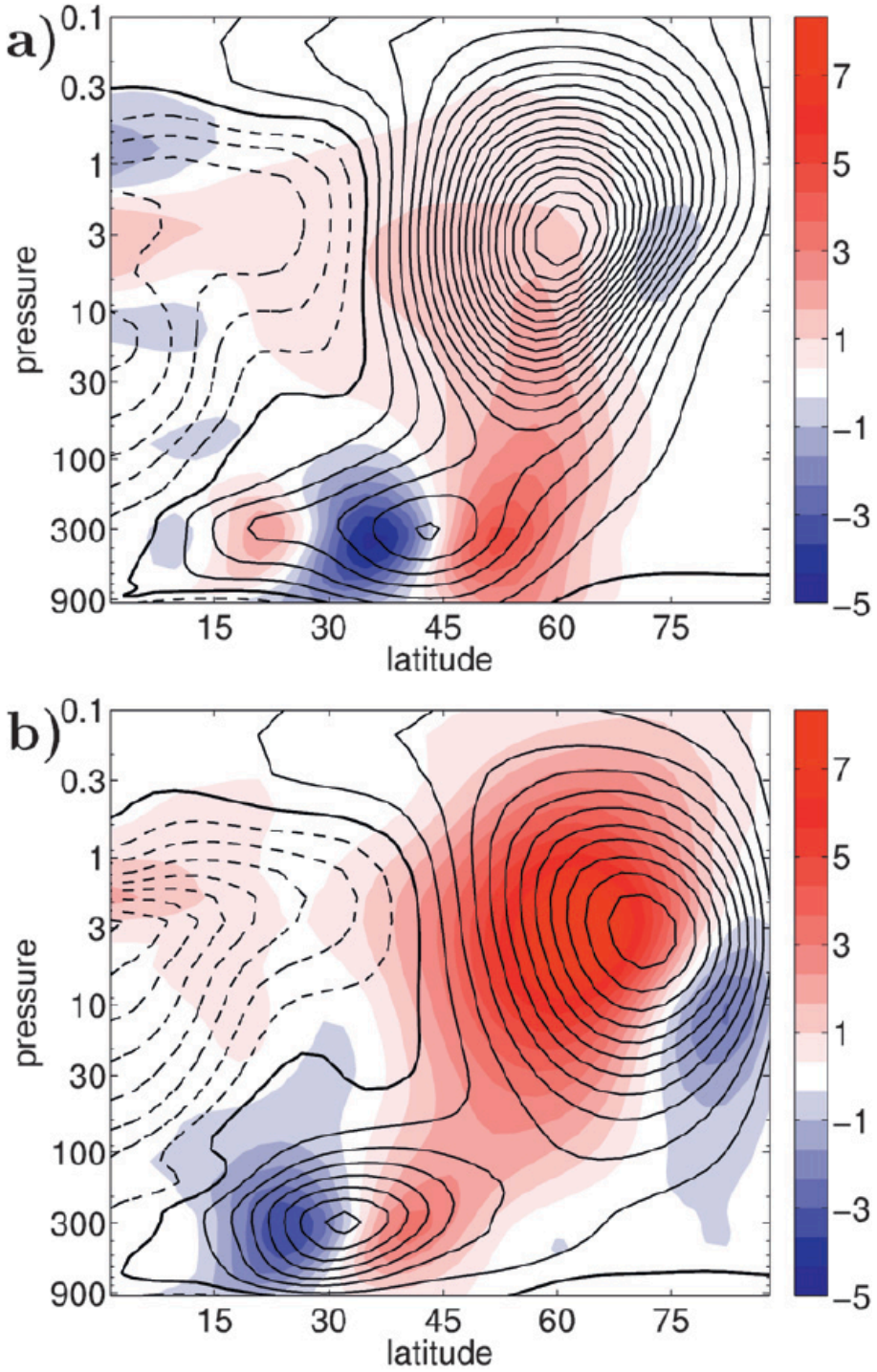

Plate 8. Climatological zonal wind (contours) and regression of AM in zonal wind (shading) for two versions of a simplified GCM with the same reference temperature profile in the troposphere and stratosphere but with (a) no topography and (b) wave-2 topography of amplitude 3000 m. The topography affects the position and strength of the jets and the AM structure; the AM exhibits stratosphere-troposphere coupling representative of the active season only in the second case. From *Gerber and Polvani* [2009].

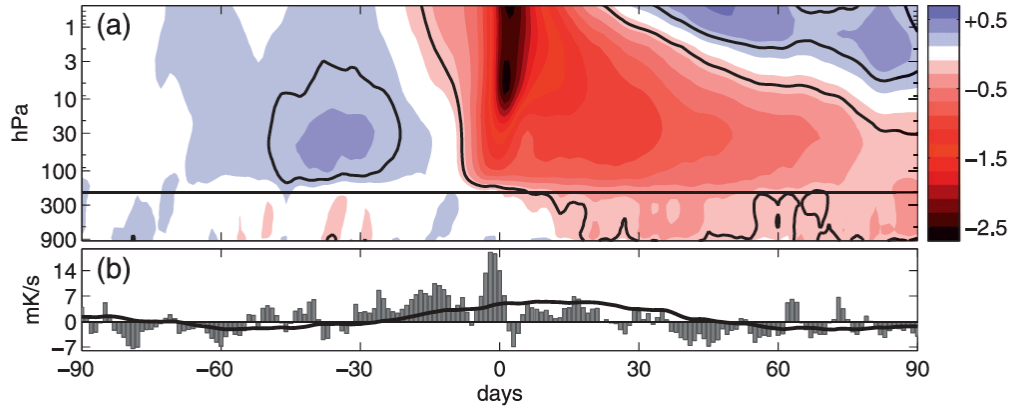

Plate 9. (a) AM index composited on strong negative NAM events in the stratosphere, which correspond to stratospheric warmings, for the simplified GCM configured as in Plate 8b. (b) Composite of a measure of the vertical component of the wave activity (bars) and its mean for the previous forty days (solid line) for the same NAM index. In the configuration where the simplified GCM has a realistic AM structure, it is able to represent downward propagating NAM events in a realistic manner, although the persistence of the NAM in the troposphere and stratosphere is generally longer than observed. From *Gerber and Polvani* [2009]

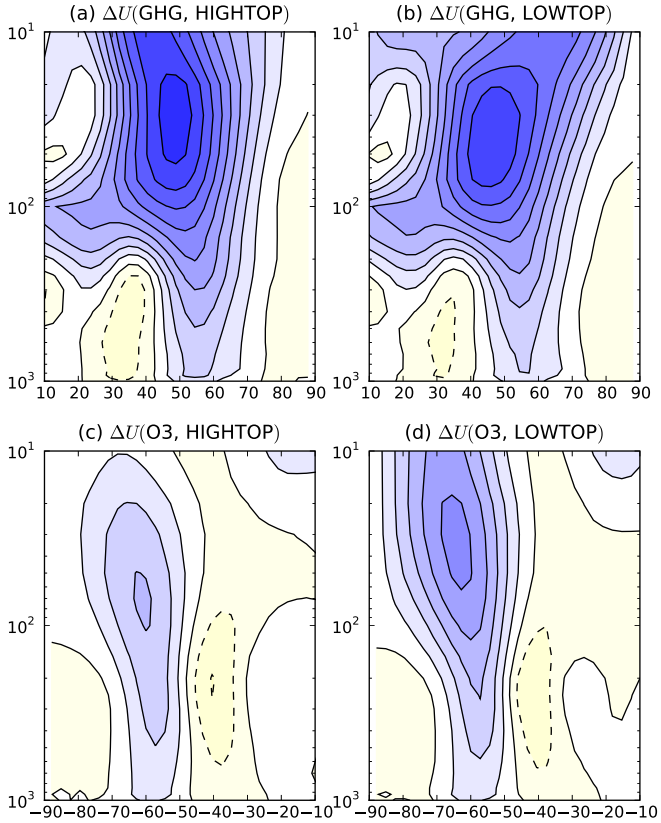

Plate 10. (a) Northern Hemisphere December-January-February zonal mean zonal wind response to CO_2 doubling in the high-top version of the Canadian Middle Atmosphere Model (CMAM) with a lid at 10^{-4} hPa. Contour interval is 1 ms^{-1} and dashed contours are negative. (b) As in (a), but for the low-top version of CMAM with a lid at 10 hPa but otherwise configured to be as consistent as possible with the high-top version. (c) Southern Hemisphere December-January zonal mean zonal wind response to Antarctic ozone depletion in the high-top CMAM. (d) As in (c), for the low-top CMAM. It is apparent that the model lid has little impact on the tropospheric AM response in these models. Adapted from *Sigmond et al.* [2008]; *Shaw et al.* [2009].